

Steinar Kragset

Phase transitions in effective lattice models for strongly correlated systems

# Abstract

In three research articles we have studied the critical properties of effective lattice models for strongly correlated electron systems by Monte Carlo simulations. A similar model is used in a fourth article for investigating thermal fluctuations of vortices in a rotating Bose–Einstein condensate. In the first part of this thesis we review the necessary background and introduce the models one by one. The last part is a collection of the papers.

**Paper I [1]:** We consider the scaling of the mean square dipole moment in a plasma with logarithmic interactions in a two- and three-dimensional system. In both cases, we establish the existence of a low-temperature regime where the mean square dipole moment does not scale with system size and a high-temperature regime does scale with system size. Thus, there is a nonanalytic change in the polarizability of the system as a function of temperature, and hence a metal-insulator transition in both cases. The relevance of this transition in three dimensions to quantum phase transitions in  $2 + 1$ -dimensional systems is briefly discussed.

**Paper II [2]:** The existence of a discontinuity in the inverse dielectric constant of the two-dimensional Coulomb gas is demonstrated on purely numerical grounds. This is done by expanding the free energy in an applied twist and performing a finite-size scaling analysis of the coefficients of higher-order terms. The phase transition, driven by unbinding of dipoles, corresponds to the Kosterlitz-Thouless transition in the 2D XY model. The method developed is also used for investigating the possibility of a Kosterlitz-Thouless phase transition in a three-dimensional system of point charges interacting with a logarithmic pair-potential, a system related to effective theories of low-dimensional strongly correlated systems. We also contrast the finite-size scaling of the fluctuations of the dipole moments of the two-dimensional Coulomb gas and the three-dimensional logarithmic system to those of the three-dimensional Coulomb gas.

**Paper III [3]:** We perform large-scale Monte Carlo simulations on an effective gauge theory for an easy plane quantum anti-ferromagnet, including a Berry phase term that projects out the  $S = 1/2$  sector. Without a Berry phase term, the model exhibits a phase transition in the 3DXY universality class associated with proliferation of gauge-charge neutral  $U(1)$  vortices. The instantons that

eliminate the phase transition in the gauge-charged sector are cancelled by the Berry phases. The result is a first order phase transition. This gauge theory therefore does not exhibit deconfined criticality.

**Paper IV [4]:** We perform Monte Carlo studies of vortices in three dimensions in a cylindrical confinement, with uniform and nonuniform density. The former is relevant to rotating  $^4\text{He}$ , the latter is relevant to a rotating trapped Bose condensate. In the former case we find dominant angular thermal vortex fluctuations close to the cylinder wall. For the latter case, a novel effect is that at low temperatures the vortex solid close to the center of the trap crosses directly over to a tension-less vortex tangle near the edge of the trap. At higher temperatures an intermediate tensionful vortex liquid located between the vortex solid and the vortex tangle, may exist.

# Acknowledgements

Asle Sudbø has been the supervisor for my graduate studies over the last four years. I am very grateful for that and for him giving me the opportunity to start this work in the first place. He was also teaching a couple of courses in my undergraduate studies, providing the right inspiration for me to enter the field of statistical mechanics.

About the time I was beginning my graduate studies Joakim Hove was in the process of ending his. He gave me thorough and essential help both on software issues and on physics in general, and during the last year I have enjoyed working with him again as he returned to a postdoctoral stay in Trondheim. Joakim is also acknowledged for proofreading this thesis.

Former graduate students Jo Smiseth and Eivind Smørgrav who both finished last year have been valuable discussion partners. Their numerous papers are important references and fundamentals for my study, as is the portfolio of Egor Babaev. Egor initiated the work of paper IV [4] and I highly appreciate his insight and crucial contributions to this. I thank Flavio S. Nogueira for coauthoring paper I and III [1, 3].

Fellow graduate students and postdocs continue to make our department a nice place to work. Kjetil Børkje is a coauthor of paper II [2] and he has helped me proofreading the chapter concerning that study. Eskil K. Dahl, Martin S. Grønsløth, Daniel Huertas-Hernando, Jacob Linder, Jan Petter Morten, Anh Kiet Nguyen, Lars Erik Walle: Thank you all for providing such a stimulating environment for discussions, work and pleasant coffee breaks.

Finally, I want to mention my friends and former class mates: Håvard Berland, Hugo Hammer, Kjetil Midthun and Geir Solgaard. Since you chose to stay in Trondheim after graduation, it was easy for me too to decide to continue here these four additional years.

The Norwegian University of Science and Technology has kindly provided the financial support for this work.

Steinar Kragset

Trondheim, September 2006



## List of papers

- Paper I:** S. Kragset, A. Sudbø, and F. S. Nogueira,  
*Metal-insulator transition in two- and three-dimensional logarithmic plasmas,*  
Physical Review Letters **92**, 186403 (2004).
- Paper II:** K. Børkje, S. Kragset, and A. Sudbø,  
*Instanton correlators and phase transitions in two- and three-dimensional logarithmic plasmas,*  
Physical Review B **71**, 085112 (2005).
- Paper III:** S. Kragset, E. Smørgrav, J. Hove, F. S. Nogueira and A. Sudbø,  
*First order phase transition in a gauge theory of  $S = 1/2$  quantum antiferromagnets,*  
cond-mat/0609336, (submitted to Physical Review Letters).
- Paper IV:** S. Kragset, E. Babaev, and A. Sudbø,  
*Thermal fluctuations of vortex Matter in trapped Bose condensates,*  
cond-mat/0604416, (accepted for publication in Physical Review Letters).



# Contents

<b>Preface</b>	<b>1</b>
<b>1 Statistical mechanics</b>	<b>3</b>
1.1 Statistical mechanics and thermodynamics . . . . .	4
1.2 Phase transitions . . . . .	5
1.2.1 The Ising model . . . . .	6
1.2.2 Landau theory . . . . .	8
1.3 Ginzburg–Landau theory . . . . .	9
1.3.1 Lattice regularization . . . . .	10
1.3.2 The two dimensional $XY$ model . . . . .	11
1.3.3 Mapping to the two dimensional Coulomb gas . . . . .	13
<b>2 Monte Carlo simulations</b>	<b>17</b>
2.1 Monte Carlo integration . . . . .	17
2.2 Simulating thermodynamics . . . . .	18
2.2.1 The Metropolis algorithm . . . . .	19
2.3 Reweighting . . . . .	20
2.3.1 Multiple histogram reweighting . . . . .	22
2.4 Error analysis . . . . .	24
2.4.1 Correlated measurements . . . . .	24
2.5 Finite size scaling . . . . .	25
2.5.1 The third moment of the energy . . . . .	27
2.5.2 Beyond continuous transitions . . . . .	28
2.6 The Lee–Kosterlitz method . . . . .	29
<b>3 Logarithmic plasmas</b>	<b>31</b>
3.1 Strongly correlated electron systems . . . . .	31
3.1.1 The Hubbard model . . . . .	31
3.1.2 Effective lattice gauge theory . . . . .	33
3.2 Numerical studies . . . . .	35
3.2.1 Polarizability . . . . .	36
3.2.2 Numerical evidence of a BKT transition . . . . .	37



<b>4</b>	<b>Deconfined criticality</b>	<b>41</b>
4.1	Square lattice antiferromagnet . . . . .	41
4.1.1	Dualization to avoid a complex hamiltonian . . . . .	44
4.2	Monte Carlo study . . . . .	46
<b>5</b>	<b>Trapped vortex systems</b>	<b>49</b>
5.1	Trapped Bose–Einstein condensates . . . . .	50
5.2	The frustrated, nonuniform $3DXY$ model . . . . .	51
5.2.1	Vortex position average . . . . .	53
5.2.2	Modified helicity modulus . . . . .	54
5.2.3	Renormalized density . . . . .	56
	<b>Bibliography</b>	<b>59</b>

# Preface

Strong local repulsion among electrons in many-particle systems is believed to be responsible for strange physical properties like the breakdown of Landau Fermi liquid theory in certain cuprate compounds. Since the discovery of high temperature superconductivity in such materials by Bednorz and Müller in 1986, the focus has increased on strongly correlated electron systems. In order to understand the physics of these compounds, great theoretical effort has been laid down in the study of lightly doped Mott–Hubbard insulators in two spatial dimensions (2D) at zero temperature. Effective lattice field theories in  $2 + 1$  space-time dimensions can be formulated and used in classical Monte Carlo simulations to search for characteristics of transitions between various ground states in the 2D quantum mechanical model. Such phase transitions are driven by parameters like pressure or doping.

In this thesis we present Monte Carlo results for three distinct models in  $2 + 1$  space-time dimensions. In Chapter 3 and 4 we introduce the investigations of two models for various zero temperature properties of a strongly correlated electron system in two spatial dimensions. The first is a lattice gas of charge-like particles which interact through a logarithmic potential, and predicted to exhibit a phase transition of the so-called Berezinskii–Kosterlitz–Thouless type. Due to the many similarities with the classical two dimensional Coulomb gas, we perform simulations on both two and three dimensional systems. Here, a novel characterization technique is developed and tested. In the second model, we find evidence for a phase transition of first order.

The nonuniform 3DXY model that we introduce in Chapter 5 can be applied to a trapped, three dimensional Bose–Einstein condensate. In rotating such systems, remarkably large and beautiful arrays of vortices have been experimentally attainable since the last few years. We investigate their thermal fluctuations.

Chapter 1 and 2 is devoted to review the necessary background to appreciate the work we introduce in the last three chapters, and present in the four research articles [1, 2, 3, 4]. This is done by an evolution from the simple Ising model to the phenomenological Ginzburg–Landau theory for superconductivity, which can be thought of as a generic theory for the models in the included collection of papers at the end of the thesis.

The work of this thesis is a natural continuation of the previous studies in our research group, References [5, 6, 7, 8, 9], which all have benefited from the high performance supercomputing facilities at NTNU. As effective lattice theories in condensed matter physics require large amounts of computation time, access to a powerful supercomputer has been essential.

# Chapter 1

## Statistical mechanics

Resolution is an important concept in today's digital cameras. It is now common knowledge how digital pictures are put together by millions of tiny pixels, and in a given picture we want sufficiently many so that we cannot tell them apart. Zooming in will however eventually reveal the microscopic structure of pixels. A similar effect is apparent in a newspaper picture. Even though the only colors used in the printing process are black and white, the picture contains almost every shades of gray. If you look carefully, you can see tiny dots of black onto the white paper, and the density or size of these dots decide the amount of gray. Reading the news, you don't notice the dots, your eyes average over them and the white space in between, and you only see the smooth grayscale picture.

In statistical mechanics we attempt to average over microscopic details in a system with macroscopically many particles in order to obtain thermodynamic quantities such as magnetization, total energy, and heat capacity, as well as derive the relations between them. The exact origin of these quantities disappears in the averaging process, as details in a picture are smoothed out when viewed from a distance.

There are however examples where some microscopic details are not averaged out. In a system with a *critical* behaviour, the range of correlations can grow when certain values of control parameters are approached. The range can in fact diverge to infinity, and since infinity is the same on any length scale they will in principle look the same irrespective of our zoom level. Of course, a physical system has a finite size and structures within it have to be restricted to fit into those dimensions. Still, we can often consider these systems infinitely large because they are so many orders of magnitude larger than the phenomena and the scales we think of when zooming in and out. On the other hand, in computer simulations, size does indeed play an important role, and this will be discussed in the context of finite size scaling in Chapter 2.

In the following sections, we will first establish some basic relations of statistical mechanics before we proceed to the concepts of phase transitions and critical phenomena. Along the way we will encounter a few simple but important models capturing many of the features essential for the main works in this thesis.

## 1.1 Statistical mechanics and thermodynamics

The goal of statistical mechanics is basically to compute the partition function  $Z$  for a given system [10, 11, 12]. This is a weighted sum over all configurations  $\psi$  the system can be in. All the information needed to calculate the thermodynamic properties are contained in  $Z$ . The partition function can be written

$$Z = \sum_{\{\psi\}} e^{-\beta H_\psi}, \quad (1.1)$$

where  $H$  is the system's Hamiltonian and  $\beta \equiv 1/(k_B T)$ , with  $T$  the temperature and  $k_B$  the Boltzmann's constant. Knowing this sum we can derive the expectation values of essentially all thermodynamic observables  $O$ ,

$$\langle O \rangle = \frac{1}{Z} \sum_{\{\psi\}} O_\psi e^{-\beta H_\psi}, \quad (1.2)$$

by differentiations of  $Z$  with respect to various parameters in the exponent. If the system is in thermal contact with a heat reservoir which keeps the temperature fixed, the internal energy  $U$  can be calculated from the canonical partition function by

$$U \equiv \langle H \rangle = \frac{1}{Z} \sum_{\{\psi\}} H_\psi e^{-\beta H_\psi} = -\frac{\partial}{\partial \beta} \ln Z. \quad (1.3)$$

Additionally, if we hold volume  $V$  and particle number  $N$  constant, the following fundamental thermodynamic relations involving the Helmholtz free energy  $F = U - TS$ ,

$$dF = dU - TdS - SdT \Big|_{V, N \text{ constant}} = -SdT, \quad (1.4)$$

and

$$U = F + TS = F - T \left( \frac{\partial F}{\partial T} \right) = -T^2 \left[ \frac{\partial}{\partial T} \left( \frac{F}{T} \right) \right] = \left[ \frac{\partial(F/T)}{\partial(1/T)} \right], \quad (1.5)$$

can be used to express  $F$  in terms of  $Z$ . By comparison with Equation (1.3) we find

$$F = -\frac{1}{\beta} \ln Z, \quad (1.6)$$

which acts as the connection between statistical mechanics and thermodynamics.

But the partition function can also give insight into fluctuations, something classical thermodynamics can not. Energy fluctuations around a system's equilibrium value,

$$(\delta U)^2 \equiv \langle (H - \langle H \rangle)^2 \rangle = \langle H^2 \rangle - \langle H \rangle^2, \quad (1.7)$$

can be calculated from  $Z$  by subsequent differentiations as in Equation (1.3),

$$(\delta U)^2 = \frac{1}{Z} \left( \frac{\partial^2 Z}{\partial \beta^2} \right) - \left( \frac{1}{Z} \left( \frac{\partial Z}{\partial \beta} \right) \right)^2 = \left( \frac{\partial^2 \ln Z}{\partial \beta^2} \right). \quad (1.8)$$

From the definition of the heat capacity  $C_V \equiv (\partial U / \partial T)$ , we see that the fluctuations in the energy of a system can be measured through

$$C_V = \frac{1}{k_B T^2} (\delta U)^2 \equiv \langle (H - \langle H \rangle)^2 \rangle = k_B \beta^2 \left( \frac{\partial^2 \ln Z}{\partial \beta^2} \right), \quad (1.9)$$

and from now on we set  $k_B$  equal to unity for simplicity.

Generalizing slightly to having more than one temperature-like parameter, or equivalently coupling  $\gamma$ , in the partition function, we let  $\beta H \rightarrow S = \sum_{\gamma} \gamma H_{\gamma}$ . The *moments* of the energy can then be found by differentiation of the correspondingly generalized free energy  $F$ ,

$$\frac{\partial F}{\partial \mu} = - \langle H_{\mu} \rangle, \quad (1.10)$$

$$\frac{\partial^2 F}{\partial \mu \partial \lambda} = \langle (H_{\mu} - \langle H_{\mu} \rangle)(H_{\lambda} - \langle H_{\lambda} \rangle) \rangle, \quad (1.11)$$

$$\frac{\partial^3 F}{\partial \mu \partial \lambda \partial \eta} = - \langle (H_{\mu} - \langle H_{\mu} \rangle)(H_{\lambda} - \langle H_{\lambda} \rangle)(H_{\eta} - \langle H_{\eta} \rangle) \rangle. \quad (1.12)$$

The second moment Equation (1.11) with  $\mu = \lambda = \beta$  corresponds to the heat capacity. Of these moments, the third moment Equation (1.12) will in particular prove to be a valuable tool for extracting critical exponents from Monte Carlo simulations [13, 14].

## 1.2 Phase transitions

To most people, the familiar examples of phase transitions are the boiling of water and melting of ice, but the magnetic to non-magnetic transition is a standard introductory example because of its simplicity [15]. We will concentrate on this transition which is *continuous* and can take place in uniaxial ferromagnets for which a typical situation is shown in Figure 1.1 (a). The magnetization  $M$  goes continuously to zero at a *critical temperature*  $T_C$  when the temperature is increased.

If exposed to an external magnetic field  $h$ , these systems can also demonstrate the other common type of phase transitions, namely a *first order* transition as  $h$  changes sign. In Figure 1.1 (b) the solid line at  $T < T_C$  indicates a first order transition where  $M$  jumps discontinuously from a negative to a positive value

as  $h$  is increased. Also melting transitions are typically first order. Later, we will encounter yet another type, the *Berezinskii–Kosterlitz–Thouless* transition [16, 17].

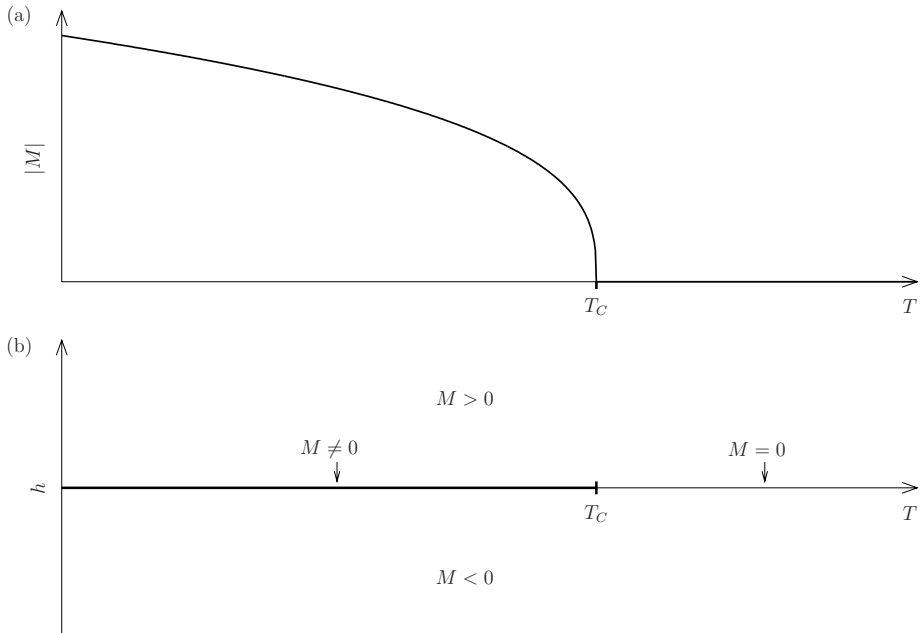


**Figure 1.1:** The magnetization  $M(T)$  goes continuously to zero at  $T_C$  (a). If an external magnetic field  $h$  is applied, the sign of  $M$  is determined by  $h$  and jumps discontinuously between a positive and a negative value across the solid line (b).

### 1.2.1 The Ising model

A uniaxial ferromagnet can be modelled on a lattice in  $d$  dimensions by the Ising model [18] given by the hamiltonian

$$H = -J \sum_{\langle ij \rangle} s_i s_j - h \sum_i s_i, \quad (1.13)$$

where  $J$  is a coupling constant determining the interaction between nearest neighbour spins  $s_i$  and  $s_j$ , and  $h$  is an external magnetic field. Each spin can point either up ( $s_i = 1$ ) or down ( $s_i = -1$ ). The lattice will in this work always be

square meaning that each spin site  $i$  has  $2d$  nearest neighbour sites. In statistical mechanics we take the temperature  $T = 1/\beta$  into account through the partition function  $Z$  Equation (1.1), and for simplicity we set the coupling  $J$  to unity, since its only effect is to define the units of  $\beta$ . If the system has the same linear extension  $L$  in units of the lattice spacing in all  $d$  directions, the number of terms in  $Z$  is  $2^{L^d}$ . Hence, the partition function is difficult and often impossible to evaluate analytically. We will get back to a way to work around this problem in Chapter 2.

In  $d = 1$  dimensions and  $h = 0$  the Ising model does not exhibit any phase transition for  $T > 0$ , but in higher dimensions it does: Consider the model in  $d > 1$  with infinitely many spins  $N \equiv L^d \rightarrow \infty$ . At high temperatures and  $h = 0$  there is no net magnetization,

$$M = \frac{1}{N} \sum_i s_i = 0, \quad (1.14)$$

because the spins are not likely to point in any particular direction. Thermal fluctuations ensure complete *disorder* among the spins. However, as the temperature is lowered the system spontaneously starts to organize a continuously growing majority of its spins either up or down when the critical temperature  $T_C$  is passed as shown in Figure 1.1 (a). Consequently, the system is said to have a *disordered* and an *ordered* phase. The two phases can be predicted from arguments regarding the free energy  $F = U - TS$ . At high temperatures  $T \rightarrow \infty$ , maximization of the entropy  $S$  will always dominate over internal energy  $U = \langle H \rangle$  in the system's quest for minimum free energy. The highest entropy is obtained by disordering the system and thus  $M(T \rightarrow \infty) = 0$ . At  $T = 0$  on the other hand, when there are no thermal fluctuations, minimizing the Hamiltonian Equation (1.13) by ordering the system so that all spins point in the same direction will minimize  $F$ . In  $d > 1$  dimensions this ordering takes place at a nonzero temperature.

In the Ising model,  $M$  is the *order parameter* describing which of the two possible phases the system is in: The disordered with  $M = 0$  or the ordered with finite magnetization. Continuous phase transitions are characterized close to  $T_C$  by a power law dependence of the order parameter on the reduced temperature  $\tau \equiv (T - T_C)/T_C$ ,

$$M \sim \tau^\beta \quad (1.15)$$

where  $\beta$  is a *critical exponent*. The order parameter is not always known in a given system, but  $\beta$  can still be found from relations to other critical exponents, see section 2.5.



### 1.2.2 Landau theory

Given that a system indeed undergoes a transition from an ordered to an un-ordered phase, Landau developed a theory describing the transition qualitatively [19]. He expanded the difference in free energy  $F$  between the two phases of the system in powers of the order parameter, keeping only the lowest order terms consistent with the symmetries of the Hamiltonian,

$$\Delta F = \frac{a\tau}{2} M^2 + \frac{u}{4!} M^4 + \dots \quad (1.16)$$

If  $h \neq 0$  in Equation (1.13), a linear term  $-hM$  has to be included, but since the theory otherwise is written down as a phenomenological effective theory, the rest of the parameters are considered free. We use the convention  $a, u > 0$ . Systems with additional intrinsic symmetries could include more terms in the expansion Eq. (1.16), such as the cubic  $M^3$ . Now, by minimizing  $\Delta F$  with respect to  $M$  the equilibrium values of the order parameter are found. From Figure 1.2 (a) we see that there is only one minimum when  $\tau$  is positive, corresponding to the high temperature phase with zero magnetization. As the temperature is decreased and  $\tau$  becomes negative, the  $M = 0$  minimum develops into two minima, and the system spontaneously chooses one of them. The up-down symmetry of the system is broken accordingly.

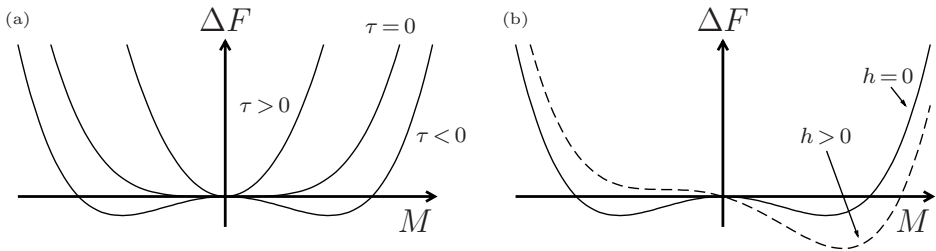


**Figure 1.2:** Difference in free energy  $\Delta F$  between to phases according to Landau theory Equation (1.16) in zero (a) and finite (b) external field  $h$ . The minima correspond to thermodynamically stable states. In (b) the reduced temperature  $\tau$  is negative.

In Figure 1.2 (b)  $\tau$  is negative, and the system can be in either of two equally probable states (solid line), but by turning on a finite  $h > 0$  there will only be one true minimum in  $\Delta F$  (dashed line). In this way the system is forced to be in a state with positive magnetization. If the system originally was in the negatively magnetized state, it will make a discontinuous jump in  $M$  corresponding to a first order phase transition.

The Landau theory does not depend on the microscopic properties of the system. The symmetries of the set of possible ordered phases is reflected in the free energy expansion Equation (1.16), but the symmetries of the true Hamiltonian is in general unknown. Additionally does the theory not depend on the lattice on which we defined the Ising model Equation (1.13). One of the strengths of the theory is that it treats correctly the importance of symmetry in the qualitative aspects of critical phenomena. In the above introduction, we had a uniaxial ferromagnet in mind, but any system with the same set of symmetries could in principle be described by the same theory. This hints to the concept of universality.

### 1.3 Ginzburg–Landau theory

The Landau theory provides a qualitative description of phase transitions, but its quantitative predictions for  $T_C$  or the critical exponents are generally wrong because the theory neglects the effect of fluctuations. A natural generalization would be to allow the magnetization to depend on position,

$$M = \frac{1}{V} \int dV m(\mathbf{r}). \quad (1.17)$$

Here, we have also allowed the space to be continuous and replaced the number of lattice sites  $N$  with the volume  $V$  of the system. The simplest extension of Landau theory to incorporate this position dependent order parameter  $m(\mathbf{r})$  and fluctuations of it, is called the *Ginzburg–Landau theory* [20],

$$\Delta F = \int dV \left[ \frac{g}{2} (\nabla m)^2 + \frac{a\tau}{2} m^2(\mathbf{r}) + \frac{u}{4!} m^4(\mathbf{r}) + \dots \right]. \quad (1.18)$$

This theory has actually proved successful, with small variations, as an *effective Hamiltonian* for many different systems. So far, we have only considered a scalar order parameter, but it could as well take a vector or a tensor to characterize the order of the given system. In a superconductor, the order parameter is the superconducting wavefunction

$$\Psi(\mathbf{r}) = |\Psi(\mathbf{r})| e^{i\theta(\mathbf{r})} = \sqrt{n} e^{i\theta(\mathbf{r})}, \quad (1.19)$$

where  $n$  is the density of Cooper pairs. Since this is a charged and quantum mechanical phenomenon, we include the electromagnetic vector potential  $\mathbf{A}$  into the gradient term in the standard way

$$\nabla \rightarrow (-i\hbar\nabla - 2e\mathbf{A}), \quad (1.20)$$

and also add a term proportional to  $|\nabla \times \mathbf{A}|^2$  in the effective hamiltonian. The full Ginzburg-Landau theory for a superconductor reads

$$H_{SC} = \int dV \left[ \frac{g}{2} |(\nabla - i\mathbf{A})\Psi(\mathbf{r})|^2 + \frac{a\tau}{2} |\Psi(\mathbf{r})|^2 + \frac{u}{4!} |\Psi(\mathbf{r})|^4 + \frac{\kappa}{2} |\nabla \times \mathbf{A}|^2 \dots \right]. \quad (1.21)$$

For simplicity, we have here rescaled  $\mathbf{A}$  and the free parameters so as to absorb Planck's constant  $\hbar$  and the charge  $2e$  of the Cooper pairs.

There is actually a close connection between the statistical mechanics of Ginzburg-Landau like theories and quantum field theories in one time and  $d$  spatial dimensions at zero temperature. This can be realized by writing down the Feynman path integral of a quantum mechanical problem and interpret it as the partition function of a classical system in  $d + 1$  Euclidian dimensions [21].

### 1.3.1 Lattice regularization

The Ginzburg-Landau hamiltonian of Equation (1.21) is a continuum theory, but for the following, and especially later for the computer simulations, it is more convenient to reintroduce a lattice. That is, we let the order parameter  $\Psi(\mathbf{r}) \rightarrow \Psi_i$ , so that it is only defined on lattice sites  $i = 1, \dots, N$  separated by a lattice constant  $a$ . Now, we have to replace the gradient term with a gauge invariant lattice difference,

$$|(\nabla - i\mathbf{A})\Psi(\mathbf{r})|^2 \rightarrow \sum_{\mu} |\Psi_{i+a\mu} e^{-iA_{i\mu}} - \Psi_i|^2, \quad (1.22)$$

where  $i + a\mu$  is the lattice site situated next to site  $i$  in direction  $\mu$ . The gauge field here lives on the links of the lattice and is given by the line integral

$$A_{i\mu} = \int_i^{i+a\mu} dl A_{\mu}. \quad (1.23)$$

The continuum is recovered if we let  $a \rightarrow 0$ . For high  $T_C$  superconductors it is a well established approximation only to consider fluctuations in the phase of the order parameter [22]. In this approximation, known as the London model, we assume a condensate of Cooper pairs to exist by having a finite and constant  $|\Psi_i| = |\Psi|$ , since in the end, it is not the depletion of Cooper pairs that is responsible for destroying superconductivity. Increasing the temperature, large fluctuations in the phase  $\theta$  makes the condensate incoherent and non-superconducting before  $|\Psi|$  vanishes. The right hand side of Equation (1.22) can thus be rewritten

$$|\Psi_{i+a\mu} e^{-iA_{i\mu}} - \Psi_i|^2 = |\Psi|^2 [2 - 2 \cos(\Delta_{\mu} \theta_i - A_{i\mu})], \quad (1.24)$$

where  $\Delta_\mu \theta_i = \theta_{i+a\mu} - \theta_i$ . To further simplify the model without changing any qualitative properties, we drop constant terms in Equation (1.21) and set the amplitude  $|\Psi|$  and lattice constant  $a$  to unity. The resulting effective lattice Hamiltonian for superconductivity is

$$H_{\text{London}} = \sum_{i,\mu} \left[ -g \cos(\Delta_\mu \theta_i - A_{i\mu}) + \frac{\kappa}{2} (\varepsilon_{\mu\nu\lambda} \Delta_\nu A_{i\lambda})^2 \right]. \quad (1.25)$$

We have here rewritten the curl in terms of the totally Levi–Civita tensor  $\varepsilon_{\mu\nu\lambda}$ . By neglecting the gauge field, Equation (1.25) is nothing but the  $XY$  model, a generalization of the Ising model Equation (1.13).

### 1.3.2 The two dimensional $XY$ model

The Hamiltonian of the  $XY$  model,

$$H_{XY} = - \sum_{\langle ij \rangle} \mathbf{s}_i \cdot \mathbf{s}_j \quad (1.26)$$

is similar to the Ising model Equation (1.13), but the spins  $\mathbf{s}_i$  are now vectors of unit length, living in a continuous two dimensional spin space. Thus, the Hamiltonian can be written

$$H_{XY} = - \sum_{\langle ij \rangle} \cos(\theta_j - \theta_j) = - \sum_{i,\mu} \cos(\Delta_\mu \theta_i). \quad (1.27)$$

The model can be generalized to have a position dependent bare *phase stiffness*, which would appear as a coefficient  $P_{ij}$  in front of the cosine terms (see Chapter 5, but at this point we only consider  $P_{ij} = 1$ ). If the lattice on which the spins are situated is two dimensional ( $2D$ ), the  $XY$  model is of special interest from the perspective of phase transitions and critical phenomena because it has a transition which is neither first order nor continuous.

According to Mermin and Wagner [23], there can never be long range order at finite temperatures in two dimensional models with a continuous symmetry. Specifically, for the  $2DXY$  model the magnetization  $M = 0$  for all nonzero temperatures. At low temperatures there is quasi long range order, but at large distances smooth spin waves eventually destroy the spins' tendency to point in the same direction. The spin–spin correlations decay algebraically, a feature typical to the situation precisely at the critical temperature of a continuous phase transition. This time however, the feature applies to all temperatures below a certain value, the transition temperature  $T_{KT}$ . In the high temperature limit on the other hand, even short range order is absent due to large thermal fluctuations, and the spin–spin correlations decay exponentially with distance.

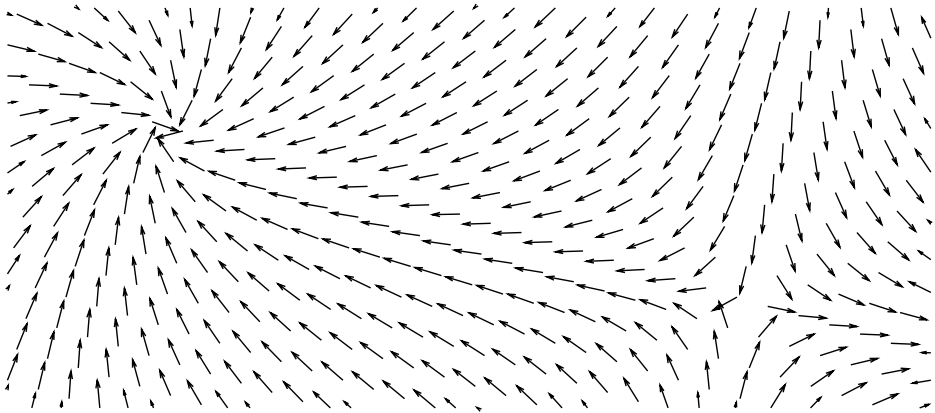


**Figure 1.3:** A pair of vortices in a two dimensional configuration of spins. The rotation of the phase is opposite around each of the two centers, hence there is no net vorticity. The pair can be viewed as a neutral configuration of charges.

Separating the critical low temperature regime, with algebraic decay of correlations, from the high temperature regime with exponential decay, there is a phase transition where *vortices* start to proliferate. Vortices are topological objects originating from the periodic nature of the phases in the Hamiltonian Equation (1.27). To characterize the vortices, we use the *vorticity*  $q$  in a region around which we integrate,

$$\oint d\mathbf{l} \cdot \nabla \theta = 2\pi q. \quad (1.28)$$

The vorticity can be viewed as a positive or negative charge, and this can actually be taken even more literally. In the next section we will demonstrate how the  $2DXY$  model with periodic boundary conditions can be mapped onto a neutral two dimensional Coulomb gas where the charges appear in pairs. A corresponding pair of vortices is shown in Figure 1.3. Since the two vortices have opposite rotation, there is no net vorticity, or charge, in this specific configuration of spins.

The phase transition we mentioned is normally referred to as the *Kosterlitz—Thouless* transition [17], and often Berezinskii is also added since he independently contributed to the understanding of the mechanism [16]: The quasi long range order at low temperatures is reflected by a finite stiffness, namely the helicity modulus  $\Upsilon_\mu$ , associated with twisting the phases. It is given by the second order derivative of the free energy with respect to the total twist  $\delta$  of the phases

across the system in  $\mu$  direction,

$$\Upsilon_\mu \equiv \left. \frac{\partial^2 F}{\partial \delta^2} \right|_{\delta=0} = \frac{1}{N} \left\langle \sum_i \cos(\Delta_\mu \theta_i) \right\rangle - \frac{1}{NT} \left\langle \left[ \sum_i \sin(\Delta_\mu \theta_i) \right]^2 \right\rangle. \quad (1.29)$$

This quantity vanishes discontinuously as vortex pairs proliferate at the phase transition. In a superfluid,  $\Upsilon_\mu$  is nothing but the superfluid density.

### 1.3.3 Mapping to the two dimensional Coulomb gas

In this section we will demonstrate a typical mapping for lattice models from a phase representation to a form in which the models are given in terms of their topological objects. Sometimes, this mapping is called a dualization, but following the terminology of Savit [24], a dualization transforms the low temperature region of a model into the high temperature region of its dual counterpart and vice versa. In our particular case of the  $2DXY$  model, this is only a part of the mapping, and the temperature in the final model is directly proportional to the temperature in the original. The topological objects are the vortices described above, and in the end we will recognize these as point particles, or charges, interacting through a Coulomb potential.

We begin with the partition function of the  $XY$  model

$$Z_{XY} = \int \mathcal{D}\theta e^{\beta \sum_{i,\mu} \cos(\Delta_\mu \theta_i)}, \quad (1.30)$$

where the phases are restricted to  $[0, 2\pi)$ . The Villain approximation [25] is applied to obtain

$$Z = \int \mathcal{D}\theta \sum_{\{n\}} e^{-\frac{\beta}{2} \sum_{i,\mu} (\Delta_\mu \theta_i - 2\pi n_{i,\mu})^2}, \quad (1.31)$$

and this is the only approximation we will make in the transformation. The integer fields  $n \in (-\infty, \infty)$  have been introduced to take care of the periodicity of the cosine. The next step is to do a Hubbard–Stratonovich decoupling where every  $n_{i,\mu}$  is decoupled from  $\Delta_\mu \theta_i$  at the prize of introducing a real valued field  $v_{i,\mu} \in (-\infty, \infty)$  in the partition function,

$$Z = \int \mathcal{D}\theta \int \mathcal{D}v \sum_{\{n\}} e^{-\sum_{i,\mu} [\frac{1}{2\beta} v_{i,\mu}^2 - i(\Delta_\mu \theta_i - 2\pi n_{i,\mu})v_{i,\mu}]}. \quad (1.32)$$

Now, we are able to calculate the sum over the integer fields, using the Poisson summation formula,

$$\sum_{n=-\infty}^{\infty} e^{2\pi i n v} = \sum_{\hat{v}=-\infty}^{\infty} \delta(v - \hat{v}), \quad (1.33)$$

so that the partition function takes the form

$$Z = \int \mathcal{D}\theta \sum_{\{\hat{v}\}} e^{-\sum_{i,\mu} [\frac{1}{2\beta} \hat{v}_{i,\mu}^2 - i\Delta_\mu \theta_i \hat{v}_{i,\mu}]}, \quad (1.34)$$

where the continuous  $v$  fields have been promoted to the integer fields  $\hat{v}$ . A partial summation and subsequent  $\theta$  integration leaves us with

$$Z = \sum'_{\{\hat{v}\}} e^{-\sum_{i,\mu} \frac{1}{2\beta} \hat{v}_{i,\mu}^2}, \quad (1.35)$$

and the constraint  $\Delta_\mu \hat{v}_{i,\mu} = 0$ , indicated by the prime in the sum, which we solve by writing  $\hat{v}_{i,\mu} = \varepsilon_{\mu\nu} \Delta_\nu \hat{h}_i$ . Note here that the new fields  $\hat{h}$  are also integer valued and that they are situated on the vertices of a *dual* lattice<sup>1</sup>. The model is now dual to the original  $2DXY$  model, but following in the footsteps of Einhorn and Savit [26, 24], we want to write  $Z$  in a form which displays explicitly the topological excitations corresponding to vortices. By again using the Poisson summation formula Equation (1.33) to replace  $\hat{h}$  with real valued fields  $h$ , we get

$$Z = \int \mathcal{D}h \sum_{\{m\}} e^{-\sum_{i,\mu} [\frac{1}{2\beta} (\Delta_\mu h_i)^2 - 2\pi i m_i h_i]}, \quad (1.36)$$

with the new integer fields  $m$ . Finally, we evaluate the integral over  $h$  and find

$$Z_{CG} = Z_0 \sum_{\{m\}} e^{-4\pi^2 \beta \sum_{i,j} m_i V(\mathbf{r}_j - \mathbf{r}_i) m_j}. \quad (1.37)$$

The interaction  $V(\mathbf{r}_j - \mathbf{r}_i)$  between the objects  $m_i, m_j$  at positions  $\mathbf{r}_i$  and  $\mathbf{r}_j$  is the two dimensional lattice Green's function given by

$$\Delta_\mu^2 V(\mathbf{r}_j - \mathbf{r}_i) = \delta_{ij}. \quad (1.38)$$

Furthermore,  $Z_0$  is the partition function of the spin waves, which decouple from the vortex excitations in this approximation. Focusing only on the qualitative features of the model's phase transition, we can safely ignore  $Z_0$  since it is the proliferation of vortex pairs that is responsible for destroying the quasi short range order.

The integer valued objects  $m_i$  in  $Z_{CG}$  correspond to the vortices in the original  $2DXY$  model Equation (1.30) and can be thought of as charges, since

---

<sup>1</sup>The dual lattice is shifted half a lattice spacing in each direction with respect to the original lattice.

$V(\mathbf{r}_j - \mathbf{r}_i)$  has the form of the Coulomb potential. To avoid divergence, we write the Coulomb gas Hamiltonian as

$$H_{\text{CG}} = 4\pi^2 \left[ \sum_{i \neq j} m_i V(\mathbf{r}_j - \mathbf{r}_i) m_j + V(0) \left( \sum_i m_i \right)^2 \right], \quad (1.39)$$

where the first sum is nonsingular. Now, we see that no configuration with  $\sum_i m_i \neq 0$  will contribute to the partition function since  $V(0) = \infty$  [27], corresponding to periodic boundary conditions in the  $2DXY$  model. In other words, only neutral configurations are possible.





## Chapter 2

### Monte Carlo simulations

In the previous chapter we only demonstrated what we in principle are able to do if we calculate the partition function  $Z$ , but we ignored the obvious difficulties with performing this calculation. Using the Ising model Equation (1.13) in two dimensions as an example, we soon run out of paper trying to write down every term in the partition function as we let the number of lattice sites increase. With 16 sites, there are  $2^{16}$  terms, but we are still far from the thermodynamic limit that we are ultimately interested in. However, this particular model is solved analytically by Onsager [28], and since most models can not be solved, the  $2D$  Ising model is frequently employed as a benchmarking model for numerical studies.

In the following we will review the numerical methods used in the studies presented in Chapters 3, 4, and 5.

#### 2.1 Monte Carlo integration

We employ Monte Carlo simulations to estimate thermodynamic quantities as in Equation (1.2), but basically Monte Carlo methods are just a set of related techniques for doing integrals. One of the simplest can be described by considering the integral  $I = \int_a^b f(x)dx$ , illustrated as the shaded area in Figure 2.1 (a). In order to estimate  $I$ , we randomly pick  $N$  values of  $x$ , uniformly distributed on the interval  $[a, b)$ . The estimator is then given by

$$I_{\text{est}} = \frac{(b-a)}{N} \sum_{i=1}^N f(x_i), \quad (2.1)$$

and it is clear that in the limit  $N \rightarrow \infty$  this will converge to the correct value of  $I$ . The rate of convergence can however be slow, for instance if  $f(x)$  is relatively small in large regions of the interval, as is the case in Figure 2.1 (b). For such a situation, a natural improvement would be to divide the interval into the subintervals  $[a, c)$

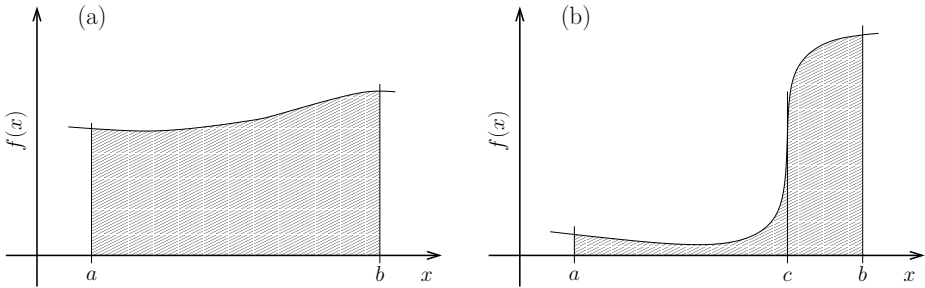


**Figure 2.1:** The definite integral of a general function  $f(x)$  from  $a$  to  $b$  illustrated as the area below the graph (a). If the function has large variations on the interval  $[a, b]$ , the integration can be divided into subintervals  $[a, c]$  and  $[c, b]$  (b).

and  $[c, b]$  and instead calculate

$$I_{\text{est}} = \frac{c-a}{N_1} \sum_{i=1}^{N_1} f(x_i) + \frac{b-c}{N_2} \sum_{i=1}^{N_2} f(y_i), \quad (2.2)$$

using  $N_1$  samples  $x_i$  from the first interval and  $N_2$  samples  $y_i$  from the second. This is a simple version of the principle called *importance sampling* where we try to sample from a nonuniform distribution favoring the most important regions in our integral. A more precise formulation of the method would be to write

$$I_{\text{est}} = \sum_i p^{-1}(x_i) f(x_i), \quad (2.3)$$

i.e. we sample from a probability distribution  $p(x)$  and weight the terms in the estimator accordingly.

## 2.2 Simulating thermodynamics

At this point we go back to our original goal, namely to estimate expectation values of thermodynamic quantities  $\langle O \rangle$  Equation (1.2). Both the partition function  $Z$  and  $\langle O \rangle$  are essentially integrals that can be estimated by the same methods as for  $I$ . The variables here are the configurations, or states,  $\psi$  consisting of many degrees of freedom and therefore making the integrals harder to estimate than  $I$  which has only one single degree of freedom,  $x$ . Still, the Monte Carlo methods

are well up to this task. The estimator takes the form

$$\langle O \rangle_{\text{est}} = \frac{\sum_i p_{\psi_i}^{-1} O_{\psi_i} e^{-\beta H_{\psi_i}}}{\sum_i p_{\psi_i}^{-1} e^{-\beta H_{\psi_i}}}. \quad (2.4)$$

If the distribution  $p_{\psi_i}$  from which we pick the sample configurations  $\psi_i$  is chosen equal to the Boltzmann weight,

$$p_{\psi_i} = e^{-\beta H_{\psi_i}}, \quad (2.5)$$

then the estimator takes the particularly simple form

$$\langle O \rangle_{\text{est}} = \frac{1}{N} \sum_i O_{\psi_i}. \quad (2.6)$$

Here, the sample distribution has cancelled the Boltzmann weights so that neither of them explicitly appear in the calculation.

### 2.2.1 The Metropolis algorithm

The next important issue in a Monte Carlo simulation is how we should efficiently generate the samples  $\psi_i$ . We do this by choosing a dynamics so that the system can evolve in discrete time steps  $t_i$  from state to state. Generally this dynamics has little in common with actual physical dynamics, it is only chosen with the purpose of effectively generating new states distributed according to  $p_{\psi_i}$ . Consequently, the *Monte Carlo time*  $t_i$  is not a physical time scale. Usually, the dynamics is also chosen so that the corresponding series of states  $\psi_i$  is a *Markov chain*, and therefore this family of methods is often called Markov chain Monte Carlo methods. A sequence of states is a Markov chain if the probability of moving to a proposed state is only dependent on that state and on the present state, and not on any of the preceding history of states. The most commonly used recipe for the dynamics is the *Metropolis–Hastings algorithm* [29], in physics normally only known as the Metropolis algorithm after its first appearance [30]. We have almost exclusively used this algorithm, however the Multicanonical sampling method [31, 32] was tried at one point during the work of chapter 4 and turned out not to be working very well with that particular model. In Figure 2.2 we summarize the Metropolis–Hastings algorithm applied to the Ising model Equation (1.13). In the algorithm, two important conditions are fulfilled for the Markov chain, namely the *accessibility assumption* and the principle of *microreversibility* [33]. The former demands that it must be possible to reach any configuration of the system from a given starting point through a finite number of iterations. Microreversibility on the other hand is the following requirement,

$$p_{\psi_k} \mathcal{P}_{\psi_k \rightarrow \psi_l} = p_{\psi_l} \mathcal{P}_{\psi_l \rightarrow \psi_k}, \quad (2.7)$$

1. In a configuration  $\psi_k$  choose a site  $i$  whose spin variable  $s_i$  is to be updated.
2. Propose a change, in this case flip the spin  $s_i \rightarrow -s_i$  to obtain a new configuration  $\psi_l$ .
3. Calculate the energy change  $\Delta H = H_{\psi_l} - H_{\psi_k}$ .
4. Calculate the acceptance probability  $\mathcal{P}_{\psi_k \rightarrow \psi_l} = e^{-\beta\Delta H}$  (if  $e^{-\beta\Delta H} > 1$ , set  $\mathcal{P}_{\psi_k \rightarrow \psi_l} = 1$ ).
5. Generate a random number  $r$  such that  $0 < r \leq 1$ .
6. If  $r \leq \mathcal{P}_{\psi_k \rightarrow \psi_l}$  accept the proposed change, else keep the initial configuration  $\psi_k$ .
7. Go to 1.

**Figure 2.2:** The Metropolis–Hastings algorithm. One iteration is called a Monte Carlo step, and going through every site in the lattice once is one Monte Carlo sweep. We define the Monte Carlo time in units of one sweep.

where  $\mathcal{P}_{\psi_k \rightarrow \psi_l}$  is the transition probability between two states  $\psi_k$  and  $\psi_l$ . This is sometimes also called *detailed balance*. The factor  $p_{\psi_k}$  is the desired probability of being in state  $\psi_k$ . Provided that  $\mathcal{P}_{\psi_k \rightarrow \psi_l}$  meets the condition Equation (2.7), it can be shown that the probability of the system being in state  $\psi_k$  at time  $t_n$  converges with increasing  $n$  to the Gibbs probability  $\exp(-\beta H_{\psi_k})/Z$ .

## 2.3 Reweighting

Temperature is normally an input parameter in our simulations, but it is not always known in advance which temperature is the most interesting. Quantities such as specific heat and the other moments of the energy (Equations (1.10–1.12)), or internal energy histograms may change dramatically as phase transitions are approached – we will encounter this behaviour repeatedly in the models investigated in this work. A helpful tool in this respect is *reweighting*, a set of techniques for utilizing fluctuations in a system around some mean at a specific temperature to gain insight into nearby temperatures [34]. It can be thought of as an advanced form for inter- and extrapolation.

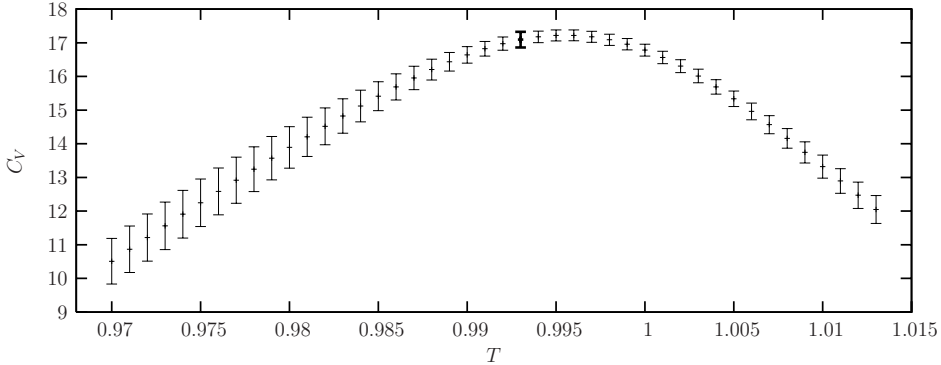


**Figure 2.3:** The heat capacity of one of the models investigated in this work. The bold data point is calculated directly from data measured during simulations at that temperature. All the other points are reweighted from that single simulation run.

The basic principle of the reweighting we have used is to store the time series (Markov chains) of energies and observables during a simulation. From Equations (1.2) and (2.6) we know how to estimate the expectation value of an observable  $O$  at the particular temperature  $T_1 = 1/\beta_1$  the simulation was run:

$$\langle O \rangle_{\beta_1} \equiv \frac{1}{Z_{\beta_1}} \sum_{\{\psi\}} O_{\psi} e^{-\beta_1 H_{\psi}} \approx \frac{1}{N} \sum_i O_i. \quad (2.8)$$

An estimate of the same observable at a slightly different temperature  $T_2 = 1/\beta_2$  can be found from the original set of data by the following derivation. Consider the somewhat strange observable  $O \exp[-(\beta_2 - \beta_1)H]$  with the expectation value

$$\langle O e^{-(\beta_2 - \beta_1)H} \rangle_{\beta_1} = \frac{\sum_{\psi} [O_{\psi} e^{-(\beta_2 - \beta_1)H_{\psi}}] e^{-\beta_1 H_{\psi}}}{Z_{\beta_1}} \approx \frac{1}{N} \sum_i O_i e^{-(\beta_2 - \beta_1)H_i}, \quad (2.9)$$

and yet another observable  $\exp[-(\beta_2 - \beta_1)H]$  with expectation

$$\langle e^{-(\beta_2 - \beta_1)H} \rangle_{\beta_1} = \frac{\sum_{\psi} [e^{-(\beta_2 - \beta_1)H_{\psi}}] e^{-\beta_1 H_{\psi}}}{Z_{\beta_1}} \approx \frac{1}{N} \sum_i e^{-(\beta_2 - \beta_1)H_i}. \quad (2.10)$$

Note that the latter equation is nothing but the ratio  $Z_{\beta_2}/Z_{\beta_1}$ . Combining Equations (2.9) and (2.10) we obtain the following estimate for  $O$  at  $T_2$ ,

$$\langle O \rangle_{\beta_2} = \frac{\sum_{\psi} O_{\psi} e^{-\beta_2 H_{\psi}}}{Z_{\beta_2}} \approx \frac{\sum_i O_i e^{-(\beta_2 - \beta_1)H_i}}{\sum_i e^{-(\beta_2 - \beta_1)H_i}}, \quad (2.11)$$

that is, an estimate based only upon measurements made at temperature  $T_1$ . An error analysis is given in the next section, but we mention briefly here that errors increase when the distance  $|\beta_2 - \beta_1|$  increases. As a rule of thumb, the energy

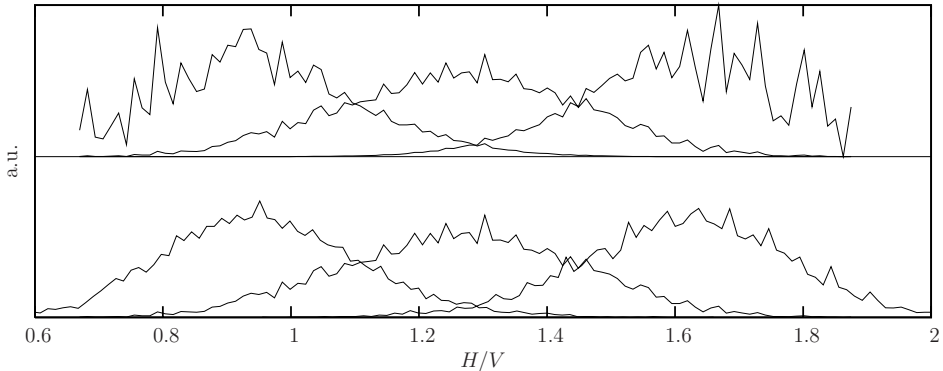


**Figure 2.4:** Energy histograms from a Monte Carlo simulation for three different temperatures. In the top panel, only the histogram in the middle is actually obtained from simulations, whereas the other two are calculated from the former through reweighting. In the lower panel, direct measurements for all three temperatures are showed.

histograms for the system at  $T_1$  and  $T_2$  should have substantial overlaps. In Figure 2.4 we see that the reweighting is satisfactory as long as the energy fluctuations of the original data provides information on the energies in the reweighted histograms. Originally the method was expressed in terms of these histograms instead of the Markov chains of  $H_i$  and  $O_i$  directly. The drawback then is that observables have to be functions of the energy, whereas in the present formulation  $H$  and  $O$  are both functions of the configuration.

### 2.3.1 Multiple histogram reweighting

In our work, we have used a more advanced version of reweighting though the underlying principles are the same. *The multiple histogram reweighting* by Ferrenberg and Swendsen [35] improves the quality of the estimates by combining data in time series obtained from simulation runs at several different temperatures, see Figure 2.5. This involves solving a set of nonlinear equations self consistently, and can be quite tricky to implement properly. Fortunately we have been provided with a software package developed by Rummukainen (first used in Reference [36]) which has been highly appreciated in several works of our research group for almost a decade.

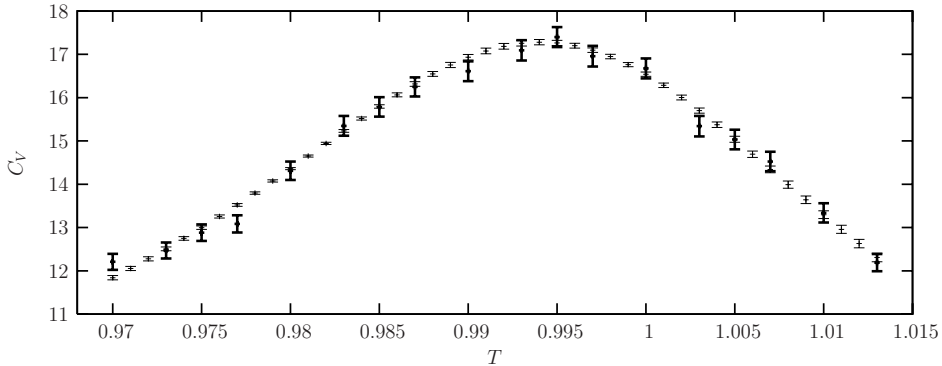


**Figure 2.5:** The heat capacity of the same system as in Figure 2.3. This time, all the bold points were simulated and combined to produce the significantly improved intermediate points by using multiple histogram reweighting.

Additionally, we have lately used a related method implemented by Hove [37], aimed at calculating the density of states  $g(H)$ , from which we can derive expectations of essentially all thermodynamic observables  $O$  as long as they can be written in terms of the energy  $H$ ,

$$\langle O \rangle_\beta = \frac{\sum_H O(H)g(H)e^{-\beta H}}{\sum_H g(H)e^{-\beta H}}. \quad (2.12)$$

The free energy is given by

$$F(T) = -T \ln \left[ \sum_H g(H)e^{-\beta H} \right], \quad (2.13)$$

and from this, moments of the energy can be derived through Equations (1.10–1.12).

In principle the two methods should yield the same results when analyzing identical Markov chains of simulation data, and they have similar limitations. A simulation performed at a given finite temperature does not provide information of the full range of energies in  $g(H)$ , and insight into which energies are covered can again be found in the energy histograms of the raw data. However, the density of states method does not fail as easy if there are insufficient overlaps between some of the raw histograms involved, as is the case in the process of solving sets of nonlinear equations in the multiple histogram method.



## 2.4 Error analysis

An important part of calculating estimates or taking measurements in physics, is to estimate corresponding errors. For a set of  $N$  uncorrelated measurements  $O_1, O_2, O_3, \dots, O_N$ , the error is just the standard error estimated from the sample variance  $S^2$ ,

$$\delta\langle O \rangle_{\text{est}} = \sqrt{S^2/N} = \sqrt{\frac{\sum_{i=1}^N (O_i - \langle O \rangle_{\text{est}})^2}{N(N-1)}}. \quad (2.14)$$

In typical Monte Carlo simulations however, the samples are highly correlated due to their originating Markov chain. The degree of correlation can be quantified through the autocorrelation function

$$\phi(t) = \frac{\langle O_{s+t} O_s \rangle - \langle O \rangle^2}{\langle O^2 \rangle - \langle O \rangle^2}, \quad (2.15)$$

where  $O_s$  is a sample taken from a simulation at Monte Carlo time  $s$ . In a Markov chain  $\phi(t)$  is proportional to  $\exp(-t/\tilde{t})$  for large  $t$ . Close to a critical point the characteristic time  $\tilde{t}$  can be very large, and in fact in the thermodynamic limit it diverges as  $T_C$  is approached. This phenomenon is known as *critical slowing down*. Large correlation times can cause problems in two respects. First of all, when we start a simulations, we want the system to *thermalize*, that is we want the system to relax and fluctuate around its global energy minimum. The number of Monte Carlo sweeps required to reach such a situation depends on the initial conditions as well as on the autocorrelation time  $\tilde{t}$ . There is no general recipe for determining the relaxation time, but a pragmatic way is to start sampling from the beginning of the simulation, and then in the post processing stage try to exclude a various number of the first samples before calculating the means. Provided that the simulation has been run for a sufficiently long total Monte Carlo time, an appropriate number of samples have been excluded when an estimate  $\langle O \rangle_{\text{est}}$  does not seem to depend appreciably on further increasing the number of excluded samples. It should be noted here that there may be more than one relaxation time in the problem. Various observables may therefore require different thermalization times.

### 2.4.1 Correlated measurements

The second problem of a large correlation time, is that the error can no longer be calculated directly from Equation (2.14). Several methods exist for taking correlations into account, but we will focus on the jackknife method [38], where the full data set of  $N$  samples is divided into  $M$  subsets  $\{\varphi_1, \varphi_2, \varphi_3, \dots, \varphi_M\}$ .

From these subsets we calculate  $M - 1$  estimates

$$\langle O \rangle_j = \frac{M}{(M-1)N} \sum_{i \notin \varphi_j} O_i \quad (2.16)$$

where the samples in subset  $\varphi_j$  are excluded from the sum. Along with the mean of the complete set,

$$\langle O \rangle_{\text{est}} = \frac{1}{N} \sum_{i=1}^N O_i, \quad (2.17)$$

we can then calculate the error estimate

$$\delta \langle O \rangle_{\text{est}} = \sqrt{\frac{M-1}{M} \sum_{j=1}^M (\langle O \rangle_j - \langle O \rangle_{\text{est}})^2}. \quad (2.18)$$

Each subset  $\varphi_j$  should contain measurements taken over a time interval much larger than  $\tilde{t}$ . A simpler method only for finding simple averages of the sampled quantities  $O$  is simply to consider the means

$$Q_j = \frac{M}{N} \sum_{i \in \varphi_j} O_i \quad (2.19)$$

of each subset as uncorrelated stochastic variables, calculate the estimator  $\langle O \rangle_{\text{est}}$  based on these  $Q_j$ , and then use the expression for sample variance Equation (2.14) with  $O$  replaced by  $Q$ . However, we often want to calculate complicated and nonlinear functions of the sampled quantities, for instance in the process of reweighting. This can be done quite straightforwardly using the estimates Equations (2.16) repeatedly as arguments of the functions, and calculating the corresponding errors of the function using Equations (2.18) this time with  $O$  replaced by the function itself.

## 2.5 Finite size scaling

Ultimately, when we do simulations we hope to apply the results to physical systems in the thermodynamic limit, but external limitation such as storage capacity and computer performance obviously limit the size of the simulated systems. Additionally there are intrinsic properties of the models that restrict us from studying too large numerical grids: The above mentioned critical slowing down in the vicinity of phase transitions grows increasingly severe when increasing the system size and there will consequently be more correlations in the Markov chain. Hence, the statistics will deteriorate due to the larger correlations, forcing

us to raise the number of Monte Carlo steps. This trade-off between large systems versus accurate statistics is always an important issue in Monte Carlo methods.

To exploit the information in results from finite systems, we do *finite size scaling*. That is, we look for scaling behaviour in observed quantities when varying the system size  $L$ . It turns out that close to critical points many thermodynamic quantities obey power-law dependence on the system size because the *correlation length*  $\xi$  diverges as  $\tau^{-\nu}$ , but is limited by  $L$  in a finite system. The exponents in these power-laws can be related to critical exponents such as  $\beta$  in Equation (1.15). Estimates of the critical exponents can in turn be used to classify the nature of a phase transition.

A full treatment of the subject should involve the renormalization group theory [39], but in the present works this has not been directly touched, and the reader is referred to the literature, see e.g. References [12, 40, 33]. Instead we turn to Widom's homogeneity postulate [41] that the singular part of the free energy  $F_s$  obeys the following relation,

$$F_s(\lambda^a \tau) = \lambda F_s(\tau), \quad (2.20)$$

where  $\lambda$  is an arbitrary scaling factor and  $a$  is an unknown constant. Since we want an expression for the scaling of  $F_s$  with respect to  $L$ , it is natural to choose  $\lambda^a = L^{1/\nu}$  to obtain the explicit  $L$ -dependence as  $\tau \rightarrow 0$ ,

$$F_s(\tau, L) = L^{1/(a\nu)} F_s(L^{1/\nu} \tau). \quad (2.21)$$

From Equations (1.9) and (1.11), we know that the heat capacity  $C_V$  is proportional to the second derivative of the free energy with respect to temperature, so the leading behaviour close to  $T_C$  can be found from

$$C_V \propto \frac{\partial^2 F_s}{\partial \tau^2} = L^{2/\nu+1/(a\nu)} \mathcal{F}(L^{1/\nu} \tau). \quad (2.22)$$

$\mathcal{F}(x)$  is just some derivative of  $F_s$  and analytical in  $x$ . The singular part of the heat capacity is normally given as  $C_V \sim |\tau|^{-\alpha}$ , and from this we identify  $a = 1/(2 - \alpha)$ . Thus, by measuring  $C_V$  at  $T_C$  for different system sizes, we can extract the ratio  $\alpha/\nu$  from

$$C_V \propto L^{\alpha/\nu}. \quad (2.23)$$

Similar scaling arguments for other thermodynamic quantities lead to a set of relations coupling the corresponding exponents, and from the *hyperscaling relation*,

$$d\nu = 2 - \alpha, \quad (2.24)$$

we can calculate  $\alpha$  and  $\nu$ . However, hyperscaling is known to be violated in certain systems [18].

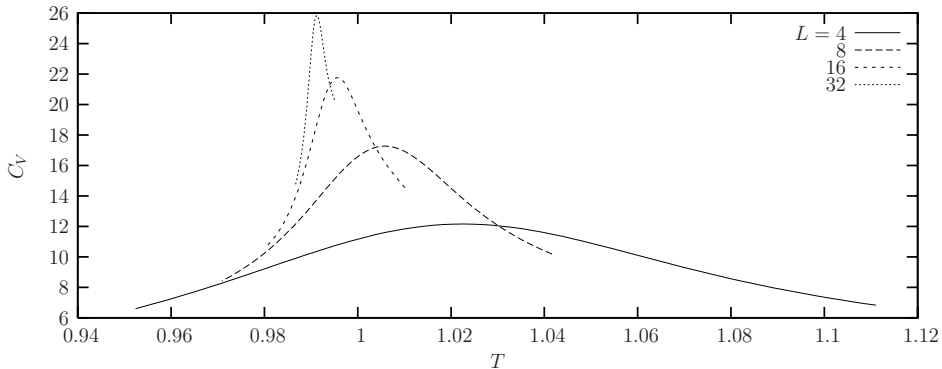


**Figure 2.6:** The heat capacity of a system with a phase transition in the  $3DXY$  universality class. Equation (2.23) predicts that the peak should be close to constant when increasing the system size, since  $\alpha$  is very small and even slightly negative. However, finite size effects in the nonsingular part of  $C_V$  obscure this behaviour for small  $L$ .

### 2.5.1 The third moment of the energy

When the  $\alpha$  exponent is close to zero, or even slightly negative as in the  $3DXY$  model<sup>1</sup>, reliable results are hard to obtain from  $C_V$  due to significant deviations from scaling in small systems. Equation (2.23) is *asymptotically* correct, but as shown in Figure 2.6, the heat capacity can actually increase with  $L$  because the analytic background dominates over the singular part for small  $L$ . In References [13, 14] Sudbø and coworkers presented a solution to this problem by, rather than computing  $C_V$ , using the third moment of the energy Equation (1.12),

$$M_3 \equiv \frac{\partial^3 F_s}{\partial \tau^3} = L^{(1+\alpha)/\nu} \mathcal{F}'(L^{1/\nu} \tau), \quad (2.25)$$

shown in Figure 2.7. Here, it is the peak-to-peak height  $(\Delta M_3)_{\text{height}}$  that scales as  $L^{(1+\alpha)/\nu}$ , and linear background terms will cancel as a result of subtraction. Additionally  $M_3$  provides a direct measure for the only length scale in the problem through the peak-to-peak *width*, which scales according to

$$(\Delta M_3)_{\text{width}} \propto \tau \sim L^{-1/\nu}. \quad (2.26)$$

The hyperscaling relation Equation (2.24) is no longer needed since  $M_3$  provides independent measures for  $\alpha$  and  $\nu$ .

<sup>1</sup>High precision measurements yield  $\alpha \simeq -0.0146(8)$  [42].

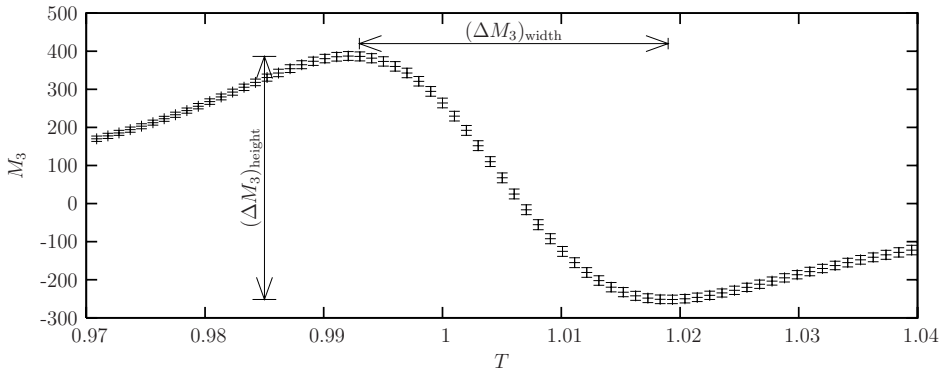


**Figure 2.7:** The third moment of the energy, corresponding to the  $L = 8$  data for the heat capacity in Figure 2.6.

## 2.5.2 Beyond continuous transitions

So far, we have only considered continuous transitions in our finite size discussion. Berezinskii–Kosterlitz–Thouless transitions are different in that there is no single temperature where the correlation length  $\xi$  diverges. Instead, we stated in section 1.3.2; the entire low temperature phase is critical, and there exists no local order parameter we can monitor. Still, a finite size analysis is useful and often the helicity modulus  $\Upsilon_\mu$  Equation (1.29) has been used to estimate the transition temperature through finite size deviations from its bulk form [43, 44]. In full analogy, the inverse dielectric constant  $\epsilon^{-1}$  has been used in the two dimensional Coulomb gas [27, 45, 46]. More conclusive evidence from Monte Carlo simulations for the very existence of a Berezinskii–Kosterlitz–Thouless in a model, is hard to find, but a novel method was proposed by Minnhagen and Kim in Reference [47]. We have further developed the method and we will come back to this in Chapter 3.

At a first order transition there are two or more noncritical phases coexisting, and no ordinary diverging correlation length is associated with the switching between them, even though quantities such as the heat capacity diverge. However, it is possible to consider first order transitions as limiting cases of continuous transitions [48, 49] where finite size scaling still makes sense. The critical exponents then attain corresponding limiting values, in particular  $\alpha = 1$  and  $\nu = 1/d$ .

## 2.6 The Lee–Kosterlitz method for first order transitions

Finite size scaling and determination of the critical exponents as described above, may give a good indication on the nature of a phase transition. Yet, a more direct approach put forward by Lee and Kosterlitz [50, 51] allows us to be more definitive about the nature of the transitions after analyzing Monte Carlo data. The idea is to identify and do finite size scaling of the domain wall energy between the coexisting phases at a first order transition. The domain walls have a surface tension corresponding to a free energy barrier  $\Delta F(L)$ , which vanishes for continuous transitions whereas it scales as  $L^{d-1}$  at a first order transition provided that  $L$  is sufficiently large.

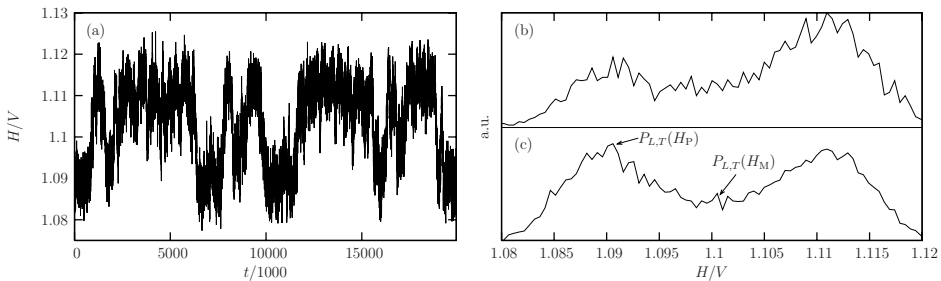


**Figure 2.8:** The Monte Carlo time series of the energy (a) indicates that there are two coexisting phases between which the system jumps. The raw histogram of the data (b) can be reweighted to a nearby temperature (c) where the two peaks are of the same height, corresponding to the transition temperature. Finite size scaling of the barrier height between the two phases will then determine the nature of the phase transition.

To calculate  $\Delta F(L)$  we again turn to the energy histograms we referred to in the context of reweighting in section 2.3, and again reweighting itself is a valuable tool. For long simulations, these histograms directly estimate the probability distribution  $P_{L,T}(H)$  for the energy  $H$  at a given system size and temperature. Two coexisting phases are reflected by two peaks in  $P_{L,T}(H)$  which are of the same height precisely at the transition temperature. Generally we do not know that exact temperature, but the histograms can then be reweighted, and from the equal height histogram  $\Delta F(L)$  can be found as

$$\Delta F(L) = \ln \left( \frac{P_{L,T}(H_P)}{P_{L,T}(H_M)} \right). \quad (2.27)$$

Here,  $H_P$  is the energy of one of the two pure states for which  $P_{L,T}(H)$  has a

maximum, and  $H_M$  is the mixed state energy corresponding to the minimum between the two peaks in the histogram as shown in Figure 2.8.

# Chapter 3

## Logarithmic plasmas in two and three dimensions

In the papers [1, 2] we study a closely related model of the Ginzburg–Landau model Equation (1.18), with focus on three dimensions arising out of a quantum mechanical problem in *two* spatial dimensions as briefly discussed in section 1.3. The study is motivated by the work in References [52, 53] where a Berezinskii–Kosterlitz–Thouless phase transition is proposed in a matter coupled compact U(1) gauge theory. This is hoped to be applicable to the proposed phenomenon of spin–charge separation in strongly correlated electron systems at zero temperature.

### 3.1 Strongly correlated electron systems

Many of the properties of high temperature superconductors can not be described by the successful theory of Bardeen, Cooper, and Schrieffer [54] for the conventional superconductors. The main issue is the strong Coulomb repulsion between the electrons with resulting breakdown of fermi liquid theory in the non superconducting phases of cuprate superconductors. For a better understanding of the cuprates, the physics of Mott insulators is considered to be crucial.

#### 3.1.1 The Hubbard model

An apparently simple model accounting for the strong electron repulsion, is the Hubbard model,

$$H = -t \sum_{\langle i,j \rangle, \sigma} C_{i\sigma}^\dagger C_{j\sigma} + U \sum_i n_{i\uparrow} n_{i\downarrow} + \text{H.c.}, \quad (3.1)$$

in the large  $U/|t|$  limit.  $C_{i\sigma}^\dagger$  and  $C_{j\sigma}$  are the usual creation and destruction operators for electrons with spin  $\sigma = \uparrow, \downarrow$ , and  $n_{i\sigma} = C_{i\sigma}^\dagger C_{i\sigma}$  is the number of electrons at lattice site  $i$  with spin  $\sigma$ . As  $U/|t| \rightarrow \infty$ , double occupancy of a lattice site is prohibited even if the electrons are of opposite spins, as illustrated in



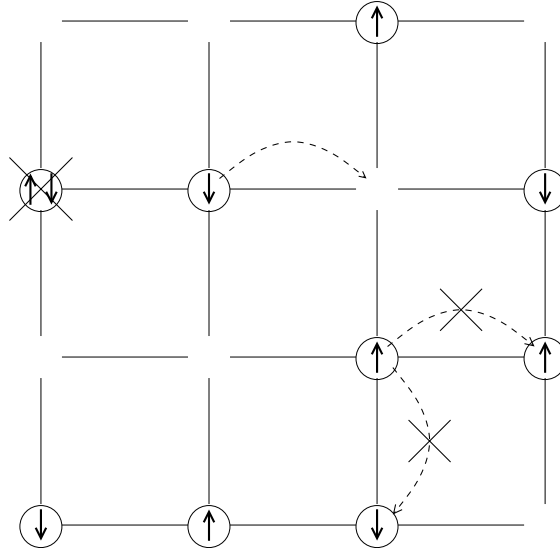


**Figure 3.1:** Possible dynamics of the large  $U/|t|$  Hubbard model. Hopping to an occupied site is not allowed even if the electrons have opposite spins.

Figure 3.1. At half filling this limit of the Hubbard model is a nearest neighbour Heisenberg antiferromagnet, believed to be an effective model for the parent compound of the cuprate superconductors,  $\text{La}_2\text{CuO}_4$ . The ground state of the system is a Mott insulator, but doping may introduce new phases. The crystal of  $\text{La}_2\text{CuO}_4$  has a layered structure of essentially independent square Cu lattices on which the low energy electron dynamics takes place [55]. In the  $U/|t| \rightarrow \infty$  limit we write the hamiltonian

$$H = -t \sum_{\langle i,j \rangle, \sigma} C_{i\sigma}^\dagger C_{j\sigma} + \text{H.c.}, \quad (3.2)$$

where we now have the additional constraint

$$\sum_{\sigma} C_{i\sigma}^\dagger C_{i\sigma} \leq 1, \quad (3.3)$$

expressing the prohibition of double occupancy. Instead of dealing with this inequality, we represent the electron operators by

$$\begin{aligned} C_{i\sigma}^\dagger &= f_{i\sigma}^\dagger b_i, \\ C_{i\sigma} &= f_{i\sigma} b_i^\dagger, \end{aligned} \quad (3.4)$$

called the slave boson method.

The operators  $f_{i\sigma}^\dagger$  and  $b_i^\dagger$  create a chargeless fermionic spin and a spinless bosonic hole respectively, and the constraint consequently takes the form of an equality,

$$Q_i|\Phi\rangle \equiv \sum_{\sigma} (f_{i\sigma}^\dagger f_{i\sigma} + b_i^\dagger b_i)|\Phi\rangle = |\Phi\rangle, \quad (3.5)$$

i.e. the site  $i$  is either occupied by a fermionic spin or else it is a positively charged hole.

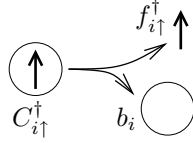


**Figure 3.2:** Slave bosonization where an electron is represented as the composite particle of a spinon carrying the spin and a holon carrying the charge.

### 3.1.2 Effective lattice gauge theory

In order to do statistical mechanics we want the partition function  $Z$ , and this we find as a Feynman path integral over Grassmann and complex fields  $f$  and  $b$  respectively [21, 56],

$$Z = \int \mathcal{D}f^* \mathcal{D}f \mathcal{D}b^* \mathcal{D}b \prod_{i,\tau} \delta(Q_i - 1) \exp \left\{ - \int_0^\beta d\tau \left[ \sum_{\langle i,j \rangle, \sigma} \left( f_{i\sigma}^* (\partial/\partial\tau) f_{j\sigma} + b_i^* (\partial/\partial\tau) b_j + \text{H.c.} \right) + H \right] \right\}, \quad (3.6)$$

where we have incorporated the constraint Equation (3.5) in the theory through the factors  $\prod_{i,\tau} \delta(Q_i - 1)$ .  $H$  is the hamiltonian of Equation (3.2) and  $\tau$  is imaginary time. We then use Abrikosov's trick of writing

$$\delta(Q_i - 1) = \int_{-\pi}^{\pi} \frac{d\lambda_i}{2\pi} e^{-i\lambda_i(Q_i - 1)}, \quad (3.7)$$

so that the partition function can be written

$$Z = \int \mathcal{D}f^* \mathcal{D}f \mathcal{D}b^* \mathcal{D}b \mathcal{D}\lambda \exp \left\{ - \int_0^\beta d\tau \left[ \sum_{\langle i,j \rangle, \sigma} \left( f_{i\sigma}^* (\partial/\partial\tau) f_{j\sigma} + b_i^* (\partial/\partial\tau) b_j + i\lambda_i(Q_i - 1) + \text{H.c.} \right) + H \right] \right\}. \quad (3.8)$$

The important feature here is that the original constraint Equation (3.3) appears in the theory in the form of a *compact gauge field*  $\lambda_i \in [-\pi, \pi)$ . After decoupling the quartic fermion terms in  $H$  by a Hubbard–Stratonovich transformation [57], the fermion sector can be integrated out. Left is a theory of a compact gauge field coupled to a bosonic field with the fundamental charge. A simplified model believed to capture the essential physics is the abelian Higgs model with a compact U(1) gauge field  $\mathbf{A}$  fundamentally<sup>1</sup> coupled to a bosonic U(1) matter field  $\Psi = |\Psi|e^{i\theta}$  defined on a Euclidian  $(2 + 1)$  dimensional lattice [58]. In the London limit, we may write the effective hamiltonian

$$H = - \sum_{i,\mu} \left[ \cos(\Delta_\mu \theta_i - A_{i\mu}) + \kappa \cos(\varepsilon_{\mu\nu\lambda} \Delta_\nu A_{i\lambda}) \right]. \quad (3.9)$$

The charge part in the underlying theory is represented by the matter field, whereas the constraint is fulfilled by fluctuations in the gauge field. We want to see if the model can support spin–charge separation in a so-called *confinement–deconfinement* transition, since a frozen gauge field would correspond to independent dynamics of the slave fermions and bosons. It should be mentioned here that this is also closely related to the issue of quark confinement in high energy physics [59].

It has long been established that a pure compact gauge theory without matter fields sustains a permanent confining phase in three dimensions [60]. Such a theory supports stable topological defects defined by surfaces where the field jumps by  $2\pi$ , forming a gas of space-time instantons. These are point like objects interacting through a  $1/r$  potential, analogous to a three dimensional Coulomb gas where the charges are always in a metallic phase due to Debye screening. If matter fields are present the fate of the instantons is however less clear. It has been argued that this does not destroy the permanent confinement [58, 59], but there has been much controversy on this point [61, 62, 63, 52, 53, 64, 65, 66, 67, 68].

In References [52, 53] a duality transformation is demonstrated for the model Equation (3.9) where the theory is expressed in terms of the gauge field instantons  $q_i$ ,

$$H = \frac{1}{2} \sum_{i,j} q_i V_{ij} q_j. \quad (3.10)$$

On a  $d = (2 + 1)$  dimensional lattice the interaction can be expressed through a discrete Fourier transformation,

$$V_{ij} \equiv V(\mathbf{r}_j - \mathbf{r}_i) = \frac{4\pi^2}{Na^d} \sum_{\mathbf{k}} \frac{e^{i\mathbf{k} \cdot (\mathbf{r}_j - \mathbf{r}_i)}}{[2(d - \sum_{\alpha=1}^d \cos k_\alpha a)]^{d/2}}. \quad (3.11)$$

---

<sup>1</sup>The *fundamental charge*  $e = 1$  is omitted but would appear in the theory in the coupling term  $\cos(\Delta_\mu \theta_i - eA_{i\mu})$ .

Here, the presence of a matter field has modified the interaction from  $\sim 1/r$  in the pure gauge theory to an anomalous  $-\ln r$  interaction in the matter coupled version. This is very similar to the *two dimensional* Coulomb gas of section 1.3.3 which is known to exhibit a Berezinskii–Kosterlitz–Thouless phase transition. Furthermore, renormalization group arguments are used to indicate that also the three dimensional logarithmic gas may undergo a phase transition of this type. A phase transition in such a system would correspond to a proliferation of space-time instantons in the gauge theory Equation (3.9). This is in turn hoped to serve as a possible mechanism for spin–charge separation through a confinement–deconfinement transition in strongly correlated systems.

As a remark, it should be mentioned that if the matter field carries a charge other than the fundamental  $e = 1$ , the situation is very different, and the model is known to have a continuous phase transition [14].

### 3.2 Numerical studies of a metal–insulator transition

The two dimensional Coulomb gas has enjoyed much attention over the last decades, see e.g. References [69, 70, 45, 27, 46, 71], and can therefore be considered as a model with well known properties. A review of the model is given in Reference [72]. Due to its similarities with our three dimensional logarithmically interacting gas of instantons, we have studied these two models simultaneously for direct comparison and benchmarking purposes. Additional comparisons with the three dimensional Coulomb gas have also been made.



**Figure 3.3:** In the two dimensional Coulomb gas, dipoles unbind in a Berezinskii–Kosterlitz–Thouless phase transition to form a metallic plasma.

Screening of the interaction potential is the essential property responsible for a phase transition in the two dimensional Coulomb gas. A finite screening length means that the system is a metallic plasma. On the other hand, since dipoles can-

not screen the Coulomb potential [73], a system initially consisting of dipoles will be in a stable dielectric phase where opposite charges are tightly bound in pairs. In two dimensions these pairs break and unbind at a finite temperature through the Berezinskii–Kosterlitz–Thouless phase transition, whereas there is only one stable phase in the *three dimensional* Coulomb gas. A permanent metallic phase in the latter model corresponds by duality to the permanent confinement of the pure U(1) gauge theory [60].

### 3.2.1 Polarizability

The theorem that dipoles cannot screen does however not apply to the *logarithmic* potential in three dimensions. This warrants numerical investigations, and in Reference [1] we use Monte Carlo simulations to investigate the screening properties of such a system. Information on this is provided by the dielectric constant, given in a low density approximation as

$$\epsilon = 1 + n_d \Omega_d p, \quad (3.12)$$

where  $n_d$  is the dipole density and  $\Omega_d$  the solid angle in a  $d$  dimensional system. The polarizability  $p$  is proportional to the mean square separation  $\langle s^2 \rangle$  between the charges in a dipole, and by focusing on this quantity in the simulations we can determine whether the system is a dielectric or a metal. For the two dimensional Coulomb gas, the behaviour of  $\langle s^2 \rangle$  to leading order in  $L$  can be found using a low density argument [17] yielding

$$\langle s^2 \rangle = \begin{cases} \text{Const.} & ; T < T_{KT} \\ aL^{(T-T_{KT})/T} & ; T_{KT} < T < 2T_{KT} \\ bL^2 & ; 2T_{KT} < T. \end{cases} \quad (3.13)$$

Here, the prefactors  $a$  and  $b$  are unimportant, whereas the constant for  $T < T_{KT}$  is of the order of the lattice constant. Even though the screening effects were neglected in this calculation, the conclusion still holds – the only correction due to screening in the above result is in value of the transition temperature  $T_{KT}$  [17]. Monte Carlo simulations confirm this behaviour in two dimensions, and the three dimensional logarithmic gas shows a remarkably similar behaviour, see Figure 3.4.

These results demonstrate clearly the existence of two different temperature regimes in the models. The scaling with  $L$  of the polarizability has a nonanalytic change at some intermediate temperature, and there must therefore be a phase transition separating the two regimes. The nature of the transition can however not be determined from the above, and further investigations are necessary. This will be presented in the next section.

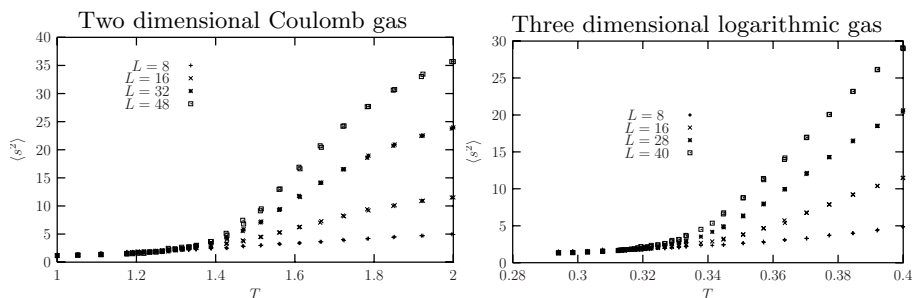


**Figure 3.4:** Results from Monte Carlo simulations showing two distinct temperature regimes in both models for the mean square dipole moment  $\langle s^2 \rangle$ .

### 3.2.2 Numerical evidence of a Berezinskii–Kosterlitz–Thouless transition

A Berezinskii–Kosterlitz–Thouless phase transition is characterized by a universal jump to zero in some generalized stiffness parameter [16, 17]. In the  $2DXY$  model, this is the helicity modulus  $\Upsilon_\mu$  (Equation (1.29)), whereas the inverse dielectric constant  $\epsilon^{-1}$  is the corresponding quantity in the two dimensional Coulomb gas. Due to the finite sizes used in computer simulations, it is diffi-

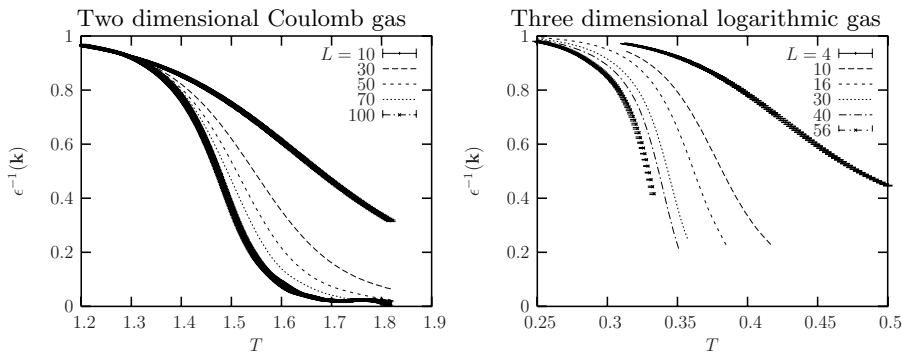


**Figure 3.5:** The inverse dielectric constant  $\epsilon^{-1}(\mathbf{k})$  as a function of the temperature  $T$ , using the smallest possible wave vector in a finite system,  $\mathbf{k} = 2\pi\hat{\mathbf{e}}_y/L$ .

cult to prove a discontinuity in  $\epsilon^{-1}$  or  $\Upsilon_\mu$  on numerical grounds. The plots in Figure 3.5 shows that the drop towards zero gets steeper as the system size is increased, but this alone does not guarantee a discontinuity in the thermodynamic limit. Yet, a simple and elegant method to prove this characteristic feature in

such phase transitions from Monte Carlo simulations, was recently put forth by Minnhagen and Kim [47]. They considered the  $2DXY$  model and its helicity modulus  $\Upsilon_\mu$ , defined by Equation 1.29. This is the coefficient of the second order term in a free energy expansion in an imposed phase twist: An arbitrarily small perturbation  $\delta$  that *increases* the free energy. Since only even order terms are nonzero in this expansion, the next term is of fourth order and the expansion can be written

$$\Delta F = F(\delta \neq 0) - F(\delta = 0) = \pi_2 \delta^2 + \pi_4 \delta^4 + \dots, \quad (3.14)$$

where  $\pi_2 \propto \Upsilon_\mu$ . The simple argument is that if the fourth order coefficient can be proven to be finite and negative at the transition temperature in the thermodynamic limit, then the helicity modulus has to be finite and positive in order to maintain stability of the system. If  $\Upsilon_\mu$  goes to zero at the transition, it necessarily cannot do so in a continuous fashion.

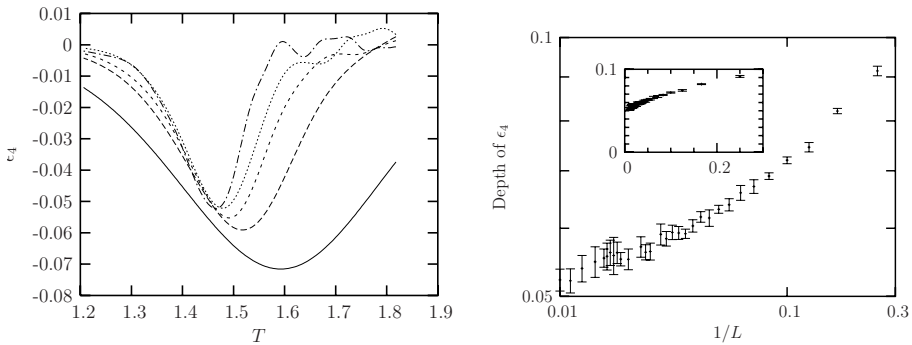


**Figure 3.6:** For the two dimensional Coulomb gas, the coefficient  $\epsilon_4$  of the fourth order term in the free energy expansion is finite and negative at the transition temperature. In the left panel  $\epsilon_4$  is plotted for increasing system size and the depth decreases monotonically with  $L$ .

We have applied the same stability argument to our logarithmically interacting plasmas in two and three dimensions, and derived the following coefficients in the corresponding free energy expansion [2]. The second order term is proportional to the inverse dielectric constant,

$$\epsilon^{-1}(\mathbf{k}) = 1 - \frac{V_{\mathbf{k}}}{L^3 T} \langle q_{\mathbf{k}} q_{-\mathbf{k}} \rangle, \quad (3.15)$$

and the fourth order term is proportional to

$$\epsilon_4(\mathbf{k}) \equiv \frac{1}{T^3} \left( \langle q_{\mathbf{k}} q_{-\mathbf{k}} \rangle^2 - \frac{1}{2} \langle (q_{\mathbf{k}} q_{-\mathbf{k}})^2 \rangle \right). \quad (3.16)$$

$V_{\mathbf{k}}$  and  $q_{\mathbf{k}}$  are the interaction and point charge respectively, given in the Fourier representation defined by  $f_{\mathbf{k}} = \sum_{\mathbf{r}} f(\mathbf{r}) \exp(i\mathbf{k} \cdot \mathbf{r})$ . Some care had to be taken in the choice of perturbation in order to make the change in free energy Equation (3.14) nondivergent as  $L \rightarrow \infty$ . In our choice  $\mathbf{k}$ , is either of the  $d$  smallest possible vectors  $\mathbf{k} = 2\pi\hat{\mathbf{e}}_{\mu}/L$  in the given system.

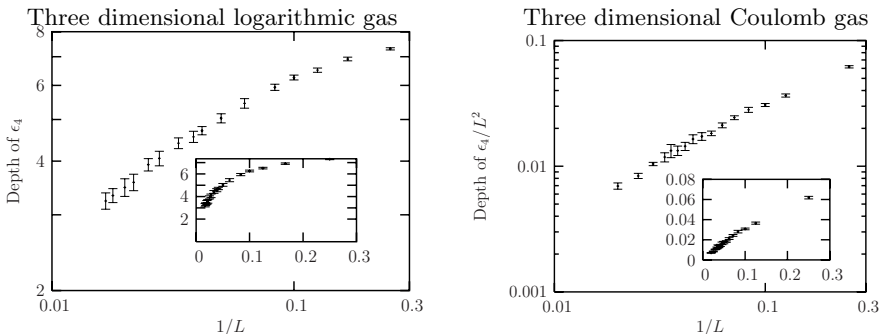


**Figure 3.7:** The depth of the fourth order coefficient vanishes in the thermodynamic limit for the *3DCG* model ( $\epsilon_4$  is divided by  $L^2$  in order to obtain the corresponding nondivergent quantity in this case). In the logarithmically interacting model, no such conclusions can be drawn.

For the two dimensional Coulomb gas, we confirm the results obtained in Reference [47]. The results (Figure 3.6) are similar to those for the *2DXY* model, and thus establish the discontinuous character of the inverse dielectric constant based on finite size scaling of  $\epsilon_4$ . The minimum of the fourth order coefficient can safely be associated with the phase transition where  $\epsilon^{-1}$  goes to zero. By plotting the corresponding temperature against  $1/L$  and extrapolating to the limit  $L \rightarrow 0$ , we can estimate the transition temperature  $T_{KT}$ , but the convergence to the known value of  $T_{KT}$  is however slow and the method is consequently not very precise.

The Berezinskii–Kosterlitz–Thouless characteristic of a discontinuous jump in the inverse dielectric constant for the three dimensional logarithmic gas can not be ruled out. Unfortunately though, the feature turns out to be hard to prove or disprove from computer simulations alone. The fourth order term has the same characteristic shape as for the *2DCG* model, and scaling of the depth is shown in Figure 3.7 along with results from simulations of the three dimensional Coulomb gas. In the latter case, the depth of the corresponding quantity  $\epsilon_4/L^2$  vanishes in the thermodynamic limit without any doubt. However, the results from the three dimensional logarithmic gas are inconclusive and either improved methods or larger system sizes are required.





# Chapter 4

## Deconfined criticality

In this chapter we use the term *deconfinement* in a somewhat different meaning than that of spin–charge separation in Chapter 3. We will however still be concerned with the physics of Mott insulators in two spatial dimensions in search for better understanding of the cuprate superconductors, but the approach will be different. Materials such as  $\text{La}_2\text{CuO}_4$  and  $\text{Cs}_2\text{CuCl}_4$  feature states with an odd number of  $S = 1/2$  spins per unit cell, but can also *dimerize* so that each unit cell consists of two  $S = 1/2$  spins, spontaneously breaking the lattice symmetry [74]. It is the dimerization of spins that in this specific context is named *confinement*. These states are paramagnetic valence bond solids and may exhibit a gap to spin excitations.

In paper [3] we study an effective model proposed by Senthil and coworkers [74, 75, 76] for the transition from a quantum Heisenberg antiferromagnet with Néel order to a dimerized spin gap state on a two dimensional square lattice. They claim that this order–order transition is continuous, in contradiction to what would be expected from the Landau–Ginzburg–Wilson framework for phase transitions. The antiferromagnetic Néel order corresponds to a broken  $\text{SU}(2)$  symmetry in spin space, whereas the valence bond solid state breaks the discrete translational symmetry in real space. According to the Landau–Ginzburg–Wilson paradigm a transition between two such ordered states must either be of first order, or there must be an intermediate disordered region. However, quantum interference effects can obscure this picture and the confining order of the two phases may be separated by a critical region where the order parameters are deconfined.

### 4.1 Square lattice antiferromagnet

The quantum Heisenberg antiferromagnet can be described by the Hamiltonian

$$H_S = J \sum_{\langle ij \rangle} \mathbf{S}_i \cdot \mathbf{S}_j + \dots \quad (4.1)$$

on a square two dimensional lattice, where  $\mathbf{S}_i$  are  $S = 1/2$  spin operators and the nearest neighbour coupling  $J > 0$ . The groundstate is the desired Néel state,

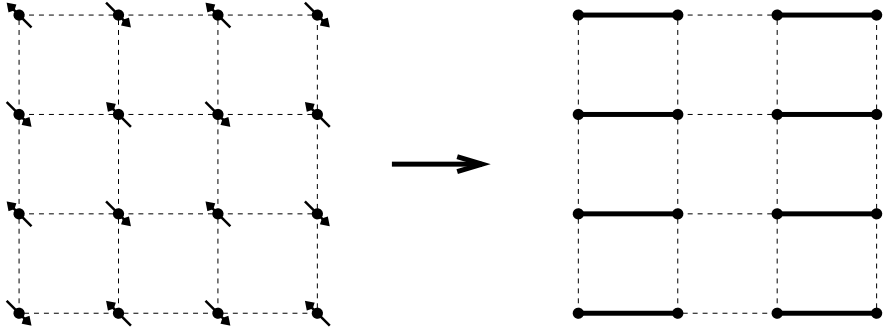


**Figure 4.1:** Schematic examples of a Néel ordered antiferromagnet and a valence bond dimer state where the discrete translational symmetry is broken.

and by adding additional terms in the Hamiltonian, it is possible to tune the system through transitions into other states such as the paramagnetic valence bond solid in Figure 4.1.

Now, a similar procedure to the one in the previous chapter can be followed to obtain an effective model for quantum fluctuations about the Néel state. It is believed that the essential physics of this system is captured by the path integral  $Z_B = \int D\theta^{(1)} D\theta^{(2)} D\mathbf{A} \exp(-H)$ , with the effective (2 + 1) dimensional Hamiltonian [74, 75, 76],

$$H = - \sum_i \left\{ \beta \sum_\mu \left[ \cos(\Delta_\mu \theta_i^{(1)} - A_{i\mu}) + \cos(\Delta_\mu \theta_i^{(2)} - A_{i\mu}) + \kappa \cos(\varepsilon_{\mu\nu\lambda} \Delta_\nu A_{i\lambda}) \right] + i2S\eta_i A_{i\tau} \right\}. \quad (4.2)$$

Here, both the phases  $\theta^{(1)}, \theta^{(2)}$  and the gauge field  $A_{i\mu}$  are compact, i.e. they are only defined on the interval  $[-\pi, \pi)$ . Even though the compact abelian Higgs model Equation (3.9) has many similarities with the above Hamiltonian, there are a few important differences to be explained. The most prominent is the so-called *Berry phase* term  $i2S\eta_i A_{i\tau}$ , accounting by a phase factor for the evolution in imaginary time  $\tau$  of each spin  $S_i$  [77, 78]. The spins are described in this theory with the identification  $\mathbf{S}_i = \eta_i S \mathbf{n}_i$ , where  $\mathbf{n}_i$  is a unit vector and  $\eta_i = \pm 1$  is a staggering factor making  $\mathbf{n}_i$  a slowly varying function of  $i$  close to the Néel ordered groundstate.  $\eta_i$  is constant in the time direction. Furthermore, in order to simplify the model, an easy-plane anisotropy is assumed so that the  $SU(2)$  symmetry of the spins is reduced to the  $U(1)$  group where spins are locked to the  $xy$  plane. The Néel vector can then be parametrized in terms of the two

component spinor  $z_i = (e^{i\theta^{(1)}}, e^{i\theta^{(2)}})/\sqrt{2}$ ,

$$\mathbf{n}_i = z_i^\dagger \vec{\sigma} z_i, \quad (4.3)$$

where  $\vec{\sigma}$  is a vector of Pauli matrices. In the limit of large  $\beta$  the partition function  $Z_B$  is dominated by configurations with small fluctuations in the phases  $\theta^{(1)}, \theta^{(2)}$ . This corresponds to the Néel ordered state with a finite  $\mathbf{n}_i$ , and  $\theta^{(1)} - \theta^{(2)}$  represents the direction of  $\mathbf{n}_i$ . The valence bond order on the other hand is connected to the factor  $\exp[-i \sum 2S\eta_i A_{i\tau}]$  in  $Z_B$ , as the Berry phases lead to a broken lattice symmetry for small  $\beta$ .

The compact gauge field of the effective Hamiltonian Equation (4.2) gives rise to the same topological defects as in the compact abelian Higgs model Equation (3.9), but now these instantons carry Berry phases. Exactly at the critical point, the combined effect of compactness and Berry phases makes the instantons cancel each other completely [74, 75, 76]. In other words, the critical theory can equally well be described by the noncompact theory

$$H = -\beta \sum_{i,\mu} \left[ \cos(\Delta_\mu \theta_i^{(1)} - A_{i\mu}) + \cos(\Delta_\mu \theta_i^{(2)} - A_{i\mu}) - \frac{\kappa}{2} (\varepsilon_{\mu\nu\lambda} \Delta_\nu A_{i\lambda})^2 \right], \quad (4.4)$$

and this argument applies to arbitrary number of components  $\theta^{(\rho)}$ .

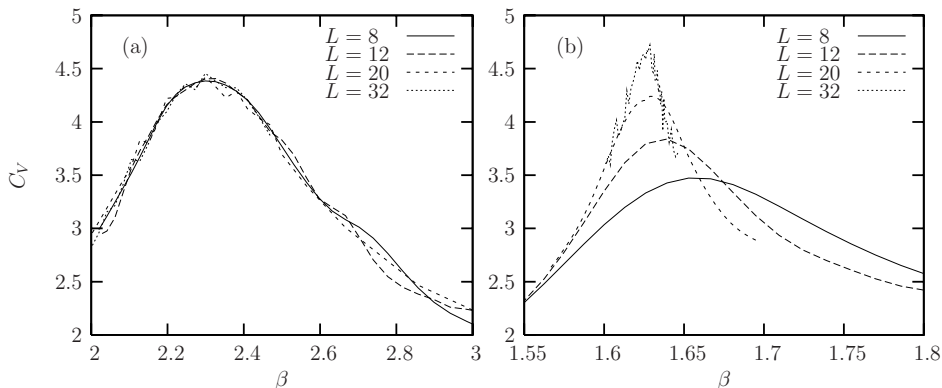


**Figure 4.2:** The peak in the heat capacity for a model with one matter field coupled to a compact gauge field does not indicate a diverging behaviour (a). If an additional Berry phase term is present (b), the heat capacity scales consistently with the  $3DXY$  model.

If we were to consider only one component, we know from the previous chapter that with a compact gauge field and no Berry phase term we get a model with no

ordinary continuous phase transition. However, if the Berry phases are included, then the critical properties would be that of the inverted  $3DXY$  universality class<sup>1</sup>. In Figure 4.2 we plot the heat capacity for the single component version of the model Equation (4.2) with and without Berry phases, and the effect is clear: The version without Berry phases shows no sign of scaling behaviour. On the other hand, for the model with the Berry phase term present, scaling of the corresponding third moment of the energy Equation (1.12) yields critical exponents in consistency with the  $3DXY$  universality class. Our main focus will be on the two component version of the model, however the same mechanism takes place: The Berry phases and instantons cancel each other at the critical point.

### 4.1.1 Dualization to avoid a complex hamiltonian

The effective model in the form of Equation (4.2) is difficult to perform Monte Carlo simulations on because it is complex. The imaginary Berry phase term may cause the partition function  $Z_B$  to contain negative terms, and consequently the normalizing factor  $1/Z_B$  in the expectation value of an observable Equation (1.2) may easily diverge. This is known as the sign problem and often encountered in quantum Monte Carlo simulations [79]. Fortunately, we are in a position where we can recast the model into a real Hamiltonian through a duality transformation akin to the one in section 1.3.3.

First we apply the Villain approximation which leaves the partition function in the form

$$Z = \int \mathcal{D}\theta^{(1)} \mathcal{D}\theta^{(2)} \mathcal{D}\mathbf{A} \sum_{\{\mathbf{n}^{(1)}, \mathbf{n}^{(2)}, \mathbf{n}^{(A)}\}} e^{-H_V}, \quad (4.5)$$

with

$$H_V = \sum_i \left\{ \frac{\beta}{2} \sum_{\mu} \left[ \left( \Delta_{\mu} \theta_i^{(1)} - A_{i\mu} + 2\pi n_{i\mu}^{(1)} \right)^2 + \left( \Delta_{\mu} \theta_i^{(2)} - A_{i\mu} + 2\pi n_{i\mu}^{(2)} \right)^2 + \kappa \left( \varepsilon_{\mu\nu\lambda} \Delta_{\nu} A_{i\lambda} + 2\pi n_{i\mu}^{(A)} \right)^2 \right] + i2S\eta_i A_{i\tau} \right\}. \quad (4.6)$$

Then we employ the standard set of tricks: The Hubbard-Stratonovich transformation and the Poisson summation formula which enable us to integrate out the  $\theta^{(1)}$  and  $\theta^{(2)}$  fields as well as the gauge field  $A_{i\mu}$ . Apparently, the partition function now becomes particularly simple,

$$Z = \sum_{\{\mathbf{v}^{(1)}, \mathbf{v}^{(2)}, \mathbf{v}^{(A)}\}} e^{-\frac{1}{2\beta} \sum_i \left( \mathbf{v}_i^{(1)2} + \mathbf{v}_i^{(2)2} + \frac{1}{\kappa} \mathbf{v}_i^{(A)2} \right)} \quad (4.7)$$

<sup>1</sup>An abelian Higgs model in three dimensions with a noncompact gauge field is dual to the  $3DXY$  model [24].

but then it must meet the following constraints,

$$\Delta \cdot \mathbf{v}_i^{(\rho)} = 0 \quad \text{where } \rho = 1, 2, \quad (4.8)$$

$$\varepsilon_{\mu\nu\lambda} \Delta_\nu v_{i\lambda}^{(A)} - v_{i\mu}^{(1)} - v_{i\mu}^{(2)} - \delta_{\mu\tau} \eta_i = 0 \quad \text{where } \mu = x, y, \tau. \quad (4.9)$$

The constraints of Equation (4.8) are fulfilled by writing  $v_{i\mu}^{(1)} = \varepsilon_{\mu\nu\lambda} \Delta_\nu h_{i\mu}^{(1)}$ ,  $v_{i\mu}^{(2)} = \varepsilon_{\mu\nu\lambda} \Delta_\nu h_{i\mu}^{(2)}$ , where  $\mathbf{h}_i^{(1)}, \mathbf{h}_i^{(2)}$  are dual lattice fields. If we additionally write the staggering term  $\delta_{\mu\tau} \eta_i$  as the curl of a new static field  $\mathbf{f}_i$ , the last constraint can be written

$$\varepsilon_{\mu\nu\lambda} \Delta_\nu \left( v_{i\lambda}^{(A)} - h_{i\lambda}^{(1)} - h_{i\lambda}^{(2)} - f_{i\lambda} \right) = 0, \quad (4.10)$$

and will be met if the parenthesis equals the gradient of a discrete scalar field  $s_i$ . Solving for  $\mathbf{v}_i^{(A)}$ ,

$$v_{i\lambda}^{(A)} = h_{i\lambda}^{(1)} + h_{i\lambda}^{(2)} + f_{i\lambda} + \Delta_\lambda s_i, \quad (4.11)$$

we end up with the real and gauge invariant *dual* partition function

$$Z = \sum_{\{\mathbf{h}^{(1)}, \mathbf{h}^{(2)}, s\}} \exp \left\{ -\frac{1}{2\beta} \sum_{i\mu} \left[ \left( \varepsilon_{\mu\nu\lambda} \Delta_\nu h_{i\lambda}^{(1)} \right)^2 + \left( \varepsilon_{\mu\nu\lambda} \Delta_\nu h_{i\lambda}^{(2)} \right)^2 + \frac{1}{\kappa} \left( h_{i\mu}^{(1)} + h_{i\mu}^{(2)} + f_{i\mu} + \Delta_\lambda s_i \right)^2 \right] \right\}. \quad (4.12)$$

The gauge invariance in Equation (4.12) allows us to choose a gauge in which the gradient term is zero and the scalar field  $s_i$  consequently is absent in the theory. In principle, we could proceed from here and express the theory in terms of its topological excitations as we did for the  $2DXY$  model, but the corresponding Hamiltonian then again turns out to be complex.

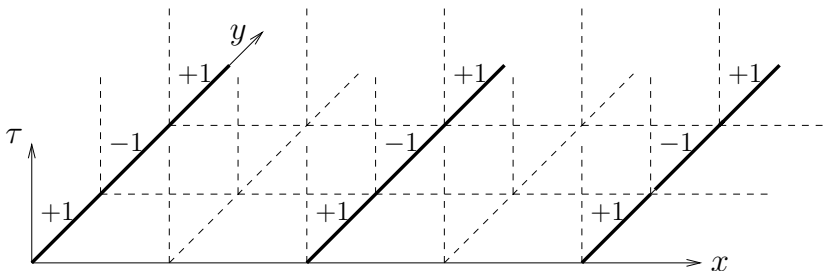


**Figure 4.3:** The components of  $\mathbf{f}_i = (f_{ix}, f_{iy}, f_{i\tau})$  are interpreted as link variables: All components are zero except for the solid links which are given the indicated values. Additionally, there is no variation in the  $\tau$  direction.

## 4.2 Monte Carlo study of a first order transition

In paper [3] we present large scale Monte Carlo simulations of the model Equation (4.12) in the  $\Delta_{\mu} s_i = 0$  gauge. This is a faithful representation of the two component effective theory Equation (4.2) for the Néel order to valence bond solid transition. Here, the Berry phases are represented by the field  $\mathbf{f}_i$ , which is defined only so that it satisfies  $\varepsilon_{\mu\nu\lambda}\Delta_{\nu} f_{i\lambda} = \delta_{\mu\tau}\eta_i$ , and we conveniently use the choice of Reference [74], see Figure 4.3.

However, by setting  $\mathbf{f}_i = 0$ , we can easily study the compact model *without* the Berry phases as well. It is known that such a theory can be rewritten in terms of a neutral mode of the  $XY$  type and a charged mode which couples to the gauge field [80, 81, 82]. Because of the compactness, the latter mode is just of the type we investigated in Chapter 3 with no continuous phase transition. Hence, we expect this theory to be in the  $3DXY$  universality class, which is in good agreement with our simulation results.

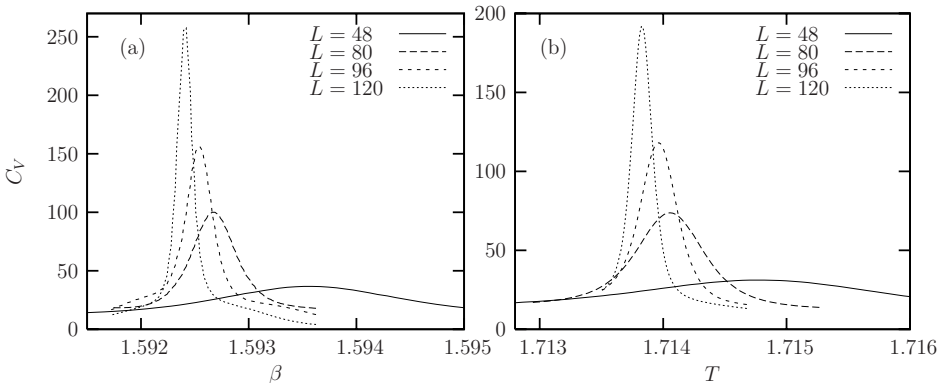


**Figure 4.4:** The heat capacity as a function of  $\beta$  or temperature respectively for the two component model with compact gauge field and Berry phases (a), and for the two component noncompact model. The symmetric peaks develop into delta functions in the thermodynamic limit, a characteristic of first order phase transitions

Finally, we perform Monte Carlo simulations on the noncompact version of the model, Equation (4.4). If the two cosine terms appear in the Hamiltonian with unequal prefactors - or phase stiffnesses - this theory is believed to be applicable to exotic systems like the Hydrogen atom at extreme pressure [83]. As in the case of a compact gauge field, we can express Equation (4.4) by a charged and a neutral mode. However this time, even the charged mode gives rise to a phase transition of  $3DXY$  type. When on the other hand the phase stiffnesses are

equal as in the present study, the theory can be shown to be *self dual* [84], in contradiction to the asymmetric  $3DXY$  phase transition.

It is argued that the critical properties of the compact model with Berry phases and the noncompact model are identical [74, 75, 76], and indeed we obtain similar results from the Monte Carlo simulations. In Figure 4.4, we see that the peaks in the heat capacity are almost perfectly symmetric in both models, and scaling of the third moment of the energy reveals practically identical critical exponents. These exponents are however surprisingly different from previous investigations [84, 82], and hint that the nature of the phase transition is not continuous, rather than *first order*. To settle this issue we have carried out a Lee–Kosterlitz analysis (see Section 2.6) and find strong evidence for a first order phase transition in these models. Thus, the peaks in the heat capacity are actually developing delta functions.





## Chapter 5

# Thermal fluctuations in trapped vortex systems

Extending the  $XY$  model from two to three dimensions, the topological objects described in section 1.3.3 becomes lines instead of points. These are vortices, objects found in systems ranging from the giant internal structure of neutron stars [85], to tiny containers of rotating superfluid  $^4\text{He}$  [86], and to extreme weather conditions like tornadoes and cyclones. In the context of high  $T_C$  superconductors, the ordering and interactions among larger numbers of vortices have been a deep and rich field of research for decades, see for example References [87, 88, 83, 89].

In certain regimes of physical parameters the  $3DXY$  model turns out to be well suited for investigations of vortex systems [90, 22, 91, 92], and the computer programs developed for the Monte Carlo studies of the last two chapters can be applied with small modifications to this problem [4]. The problem we have in mind is thermal fluctuations in arrays of vortices seen in ultracold rotating gases of bosons, the Bose–Einstein condensates. At the lowest temperatures, these arrays have a high degree of regularity [93], ordered as Abrikosov lattices, the well known form for ordering of quantized magnetic flux lines in type-II superconductors [94]. The Bose–Einstein condensates have superfluid properties, and since their experimental realization in alkali gases just over a decade ago [95, 96], they have proved to be useful testing grounds for a variety of different physical concepts. An important reason for this is that they are easily controllable in large ranges of the parameters such as total particle number, density, interparticle interaction, rotation rates and so on.

Our Monte Carlo results are believed to be applicable to harmonically trapped Bose–Einstein condensates [93] away from the extremely dilute limit of rapidly rotating systems where the rotation frequency is close to the trap frequency [97]. With small additional adjustments we have also simulated anharmonic situations where the condensate is trapped in a harmonic plus quartic potential, directly related to experiments by Bretin and coworkers [98]. Another related case is to replace the trap by a hard-walled cylinder with a uniform bare phase stiffness within, resulting in a model applicable to a rotating container of superfluid  $^4\text{He}$  [99].

## 5.1 Trapped Bose–Einstein condensates

Here, we will not review the fundamentals of Bose–Einstein condensation other than refer to a few concepts important for this work - more general introductions can be found in References [100, 101]. In order to confine the condensate atoms in space, various techniques can be used, however most experiments have a magnetic trap with axial symmetry. The potential is usually that of a harmonic oscillator and can be written

$$V(r, z) = \text{const.} + \frac{1}{2}M\omega_r^2 r^2 + \frac{1}{2}M\omega_z^2 z^2, \quad (5.1)$$

where  $M$  is the single particle mass and  $\omega_r$  ( $\omega_z$ ) is the radial (axial) oscillator frequency. By tuning the ratio  $\omega_r/\omega_z$ , the shape of the system can be manipulated. We will consider elongated systems where the cloud of condensed atoms have a cigar shape, with extension  $Z$  in  $z$  direction a few times larger than the radial extension  $R$ . In certain setups the cloud can take the form of a pancake, leaving the physics essentially two dimensional, but in the present study  $3D$  effects are important.

The size of the cloud can be estimated by simple energy considerations. In a system of  $N$  atoms rotating around the  $z$  axis with an angular rotation frequency  $\Omega$ , the rotating frame energy is

$$E_{\text{cloud}} \sim \frac{1}{2}M(\omega_r^2 - \Omega^2)R^2N. \quad (5.2)$$

In order to maintain stability, this must be comparable to the total interaction energy

$$E_{\text{int}} \sim gnN, \quad (5.3)$$

with  $g = 4\pi a_s \hbar^2/M$  the interaction strength and  $n$  the condensate density. Here is  $a_s$  the low energy s-wave scattering length. Assuming for simplicity a cubic system, then  $n = N/R^3$ , and we get

$$E_{\text{cloud}} \sim E_{\text{int}} \quad (5.4)$$

$$\Rightarrow R \sim \left[ \frac{gN}{M(\omega_r^2 - \Omega^2)} \right]^{1/5}. \quad (5.5)$$

We see that when the rotation rate approaches the trap frequency, the system flies apart and other trapping methods are necessary to confine the atoms, see for example Reference [98]. Otherwise, changing the total number of atoms in the trap offers great flexibility for controlling the size and density of the system. If  $N$  is sufficiently large, the Thomas–Fermi approximation can be applied to give the following radial density distribution of the atoms [101],

$$n(r) = n(0) \left( 1 - (r/R)^2 \right). \quad (5.6)$$

Close to  $r = R$  where the density is small, the approximation is not good and the condensate vanishes more smoothly than predicted by Equation (5.6). In a rotating system where vortices appear, the density profile  $n(r)$  must be viewed as the coarse grained density since a vortex core corresponds to a complete depletion of the condensate. The vortex core size is of the same order of magnitude as the healing length,  $\xi \sim \hbar/\sqrt{gnm}$ .

Typical experiments with Na or  $^{87}\text{Rb}$  may have  $N$  in the range of  $10^5$ - $10^7$  atoms, and trapping frequency of the order 100 Hz. For example, in Reference [93] this yields systems of up to 130 vortices with cloud size  $R \sim 29\mu\text{m}$  and healing length  $\xi \sim 0.2\mu\text{m}$ .

## 5.2 The frustrated, nonuniform 3DXY model

In paper [4] we present results obtained by Monte Carlo simulations of a frustrated 3DXY model with a position dependent, but fixed, bare phase stiffness. The *uniform* 3DXY model has been used extensively for over a decade in the context of high  $T_C$  superconductors [90, 22, 91, 92] and is assumed to work well when the average vortex separation is larger than the healing length  $\xi$ . On the contrary, when the vortex cores start to overlap as in very rapidly rotating Bose–Einstein condensates, the systems enter the lowest Landau level regime [102, 103] and the 3DXY model does not apply. This happens when the interaction energy is much smaller than the harmonic trap energy.

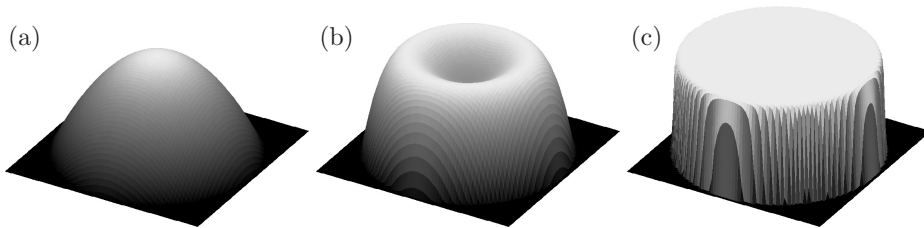


**Figure 5.1:** Various radial density distribution  $P_{ij}$  used in our simulations: With a harmonic trap (a), an anharmonic trap with a harmonic plus a quartic term (b), and a hard-walled cylindrical container (c).

We use a Hamiltonian which is a generalization of Equation (1.27) and can be written

$$H = - \sum_{\langle ij \rangle} P_{ij} \cos(\theta_j - \theta_i - A_{ij}). \quad (5.7)$$

The bare phase stiffness  $P_{ij}$  can be chosen so as to represent the Thomas–Fermi

density profile of a harmonically trapped Bose–Einstein condensate,

$$P_{ij} = \begin{cases} \left(1 - (r_{ij}/R)^2\right) & \text{when } r_{ij} \leq R, \\ 0 & \text{when } r_{ij} > R, \end{cases} \quad (5.8)$$

where  $r_{ij}$  is the radial distance from the  $z$  directed trap center axis. However, as far as the simulations are concerned, we can equally well choose other profiles, see Figure 5.1. The gauge field  $A_{ij}$  in Equation (5.7) is kept fixed during the simulations, and serves as a uniform frustration which induces a certain number of vortices in the system corresponding to some fixed rotation frequency  $\Omega$ . It is defined by

$$A_{ij} = \int_i^j d\mathbf{l} \cdot (2\pi f x \hat{\mathbf{e}}_y), \quad (5.9)$$

and in a cubic  $L \times L \times L$  lattice, there will consequently be  $fL^2$  vortex lines penetrating the system parallel to the  $z$  axis. The position of these vortices are

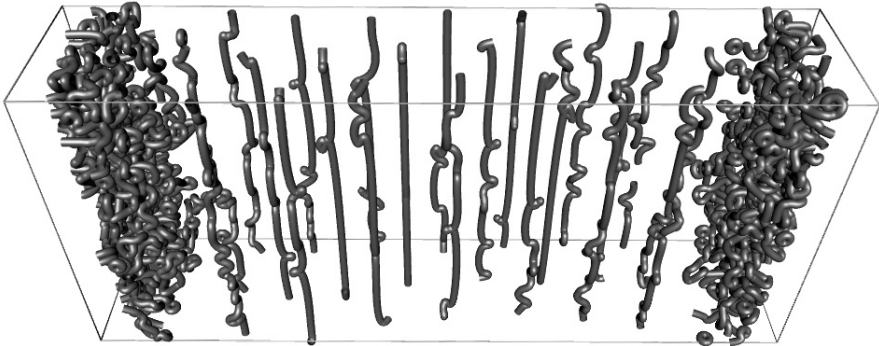


**Figure 5.2:** A snapshot of the vortices in a  $72 \times 72 \times 72$  system at  $T = 0.5$ , where the selection consists of 72 lattice spacings in  $x$  direction, 16 in  $y$  direction, and 32 in  $z$  direction. In the central part there are small fluctuations and the vortex lines are almost straight objects, whereas fluctuations increase and vortex loops eventually proliferate closer to the edge. The radius of the vortices is 0.4 times the lattice spacing, only *chosen* so for visualization reasons, and should not be compared to the physical size of the vortex cores.

determined by calculating around each plaquette  $\square_k$  the sum

$$\sum_{\square_k} (\theta_j - \theta_i - A_{ij}) = 2\pi n_k, \quad (5.10)$$

where the integer  $n_k$  is the number of vortices penetrating that particular plaquette in the positive direction. Fluctuations of the phases  $\theta_i$  are responsible for

the dynamics of the vortex lines, but can also cause the creation of closed vortex loops in the system. High temperature favours fluctuations and so the amount of vortex *loops* increase with increasing temperature. Since temperature appears in the partition function only through the prefactor  $\beta = 1/T$ , we can view the total prefactor  $\beta P_{ij}$  as an effective, position dependent inverse temperature. Hence, in the trapped system we expect large vortex fluctuations close to the edge and gradually more of a low temperature phase in the central parts. In Figure 5.2 a snapshot of a typical vortex configuration is shown for a relatively small  $T$ . Surface effects where the vortex lines leave or enter the system are ignored in this study by use of periodic boundary conditions. A cubic model system can therefore be considered as a section of an elongated cloud.

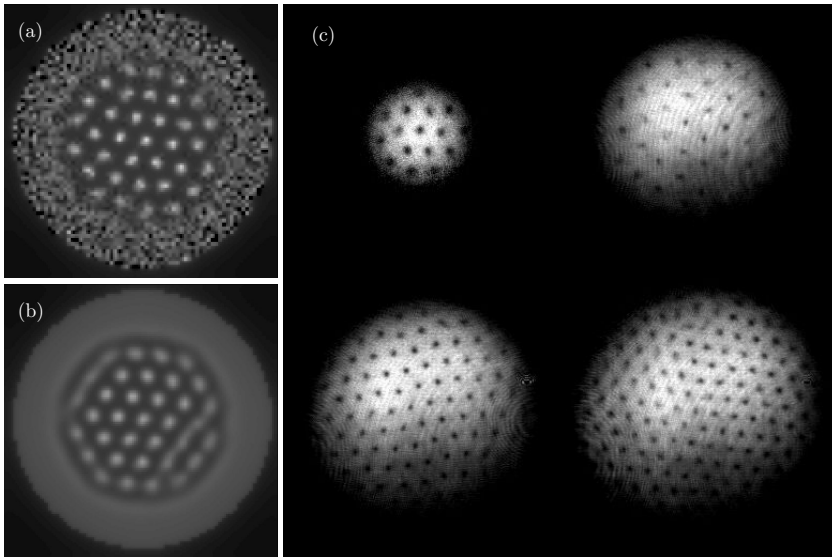


**Figure 5.3:** The vorticity in a simulation snapshot, integrated along the  $z$  direction (a). In (b) such snapshots are averaged over every tenth of  $5 \cdot 10^5$  Monte Carlo sweeps in order to produce a thermal average. Experimental pictures (c) usually reflects density variations in the cloud, and vortices are only indirectly visible through the absence of the condensate. Image courtesy (c) Wolfgang Ketterle [104].

### 5.2.1 Vortex position average

We want to monitor how the presence of a harmonic trap affects the vortex fluctuations and use Monte Carlo simulations on the nonuniform  $3DXY$  model

Equation (5.7) to produce snapshots of vortex configurations. Normally, Monte Carlo simulations are used to calculate thermal averages from large numbers of configurations. Now however, we hope to mimick the experimental situation in which the pictures indeed are snapshots.

For a given vortex configurations, we integrate the vorticity over the  $z$  direction and in this way obtain two dimensional visualizations of the three dimensional vortex systems. An example is shown in Figure 5.3 (a). In such a picture, two closed vortex loops situated on top of each other will cancel out if they are opposite in direction. On the other hand, straight vortex *lines* will be sharply defined spots, with bent lines being more smeared out regions. The main difference of these pictures from most of the pictures taken in experiments (see e.g. Figure 5.3 (c)), is that the intensity in the latter reflects local density variations in the condensate cloud, whereas in the simulated pictures, it is the vortex matter that is visualized. In real systems, vortices correspond to depletion of the condensate density and are thus only indirectly visible. Still, both visualizations provide information on the vortex position.

However, an additional feature of the simulation pictures, is that we can also do thermal averages of vortex configurations. Then, large phase fluctuations will correspond to many closed vortex loops effectively cancelling each other out, leaving behind only the sample penetrating vortex lines. Stable vortex lattice regions will remain clear in such pictures, whereas in molten regions where the vortex lines can move, the pictures will be blurred as shown in Figure 5.3 (b).

## 5.2.2 Modified helicity modulus

In the pictures of the above section, we notice a rather sharp boundary between the ordered vortex line lattice and the disordered region outside, possibly a molten phase. In order to investigate this boundary we employ a modified version of the helicity modulus  $\Upsilon_\mu$ . From investigations on high  $T_C$  superconductors, it is known that the superconducting to normal transition can be characterized by the vanishing of the helicity modulus: When vortex lines are present,  $\Upsilon_z$  is discontinuous because the vortex line lattice melts in a first order phase transition [22, 92]. The helicity modulus is proportional to the superfluid density  $\rho_s$ , and can be defined in a uniform system as the lowest order response in the free energy with respect to an infinitesimal phase twist across the system in  $\mu$  direction. In that sense,  $\Upsilon_\mu$  can be considered as the measure of an effective phase stiffness, renormalized by vortex fluctuations. Since the free energy is a global quantity,  $\Upsilon_\mu$  has no rigorous meaning in the trapped system where the bare phase stiffness  $P_{ij}$  depends on position. Nevertheless, we introduce a modified helicity modulus  $\tilde{\Upsilon}_z$  only defined between two cylinders of radii  $R_1$  and  $R_2$ . We do so by applying

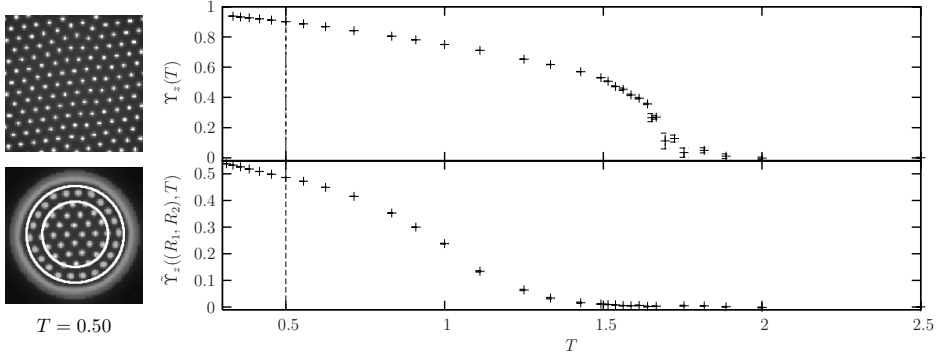


**Figure 5.4:** A comparison between the ordinary helicity modulus  $\Upsilon_z$  of a uniform system with vortex lines (top row), and the modified version  $\tilde{\Upsilon}_z$  (lower panel). The radii  $R_1$  and  $R_2$  for which  $\tilde{\Upsilon}_z$  is calculated, are indicated by the white circles in the picture on the left. Due to the larger effective temperature  $1/(\beta P_{ij})$  in this region, the stiffness vanishes at lower  $T$  than in the uniform system.

a twist

$$\Delta(r_{ij}) \equiv \Delta_{ij} = \begin{cases} \Delta \hat{\mathbf{e}}_z & \text{if } R_1 \leq r_{ij} < R_2, \\ 0 & \text{otherwise,} \end{cases} \quad (5.11)$$

to the model Eq. (5.7) to get a twist dependent energy function

$$H_{\text{trap}}(\Delta) = - \sum_{\langle ij \rangle} P_{ij} \cos(\theta_j - \theta_i - A_{ij} - \frac{1}{L} \Delta_{ij} \cdot \hat{\mathbf{e}}_{ij}), \quad (5.12)$$

where  $\hat{\mathbf{e}}_{ij}$  is the unit direction vector of link  $ij$ . The cylinder version of the helicity modulus can then be defined

$$\begin{aligned} \tilde{\Upsilon}_z(R_1, R_2) \equiv \frac{\partial^2 F'}{\partial \Delta^2} \Big|_{\Delta=0} &= \frac{1}{N'} \left\langle \sum' P_{ij} \cos(\theta_j - \theta_i - A_{ij}) \right\rangle \\ &- \frac{1}{TN'} \left\langle \sum' \left[ P_{ij} \sin(\theta_j - \theta_i - A_{ij}) \right]^2 \right\rangle \end{aligned} \quad (5.13)$$

where  $\sum'$  is over all links where  $\Delta_{ij}$  is nonzero (depends on  $R_1$  and  $R_2$ ) and  $N'$  is the number of these links. The total free energy  $F$  of the system will have contributions due to the large gradient in the phase twist normal to the surfaces defined by  $R_1$  and  $R_2$ , and we therefore *choose* only to calculate the response in free energy  $F'$  for the subsystem between the two surfaces. It is clear that in the



limit where the volume of this subsystem goes to infinity,  $\tilde{\Upsilon}_z$  converges to  $\Upsilon_z$ . Yet, we also believe that the modified helicity modulus is a useful probe of the states in a finite system. This is further discussed in paper [4].

### 5.2.3 Renormalized density

An alternative way of visualizing the vortex lattice is to create two dimensional plots similar to those in Section 5.2.1, but this time integrating *density* rather than vortex positions. The density is estimated simply by associating the underlying lattice constant of the numerical grid with the vortex core size: A unit cell in the grid has density  $1/L$  if it is empty and 0 if it is penetrated by a vortex. This we integrate along the  $z$  direction and modulate with the a priori density given by  $P_{ij}$ . The resulting two dimensional plots now provides information both on the vortex line lattice structure and on the density of the condensate cloud itself, renormalized by vortex fluctuations.

This is directly comparable to the experimental pictures, and in particular, we consider [105] results from experiments performed by Bretin and coworkers [98]. They used a trap with an additional quartic term in order to confine the atoms

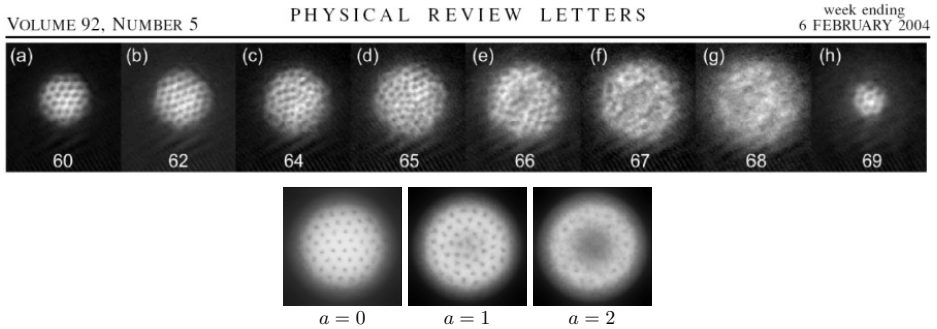


**Figure 5.5:** Observation of vortices in an experiment where the condensate was confined by a harmonic plus quartic potential (top row), after Bretin and coworkers [98]. Renormalized condensate density from simulations with a similar density profile is shown in the bottom row. Note the loss in visibility when the strength of the harmonic term increases, corresponding to faster rotation relative the trap frequency.

even when approaching the harmonic trap frequency  $\omega_r$ . An unexplained feature in their results was the loss in visibility of the vortices at high rotation rates (see Figure 5.5), which we believe is due to the reduced density in the central parts of the cloud. Such a reduction is readily interpreted as an increased effective

temperature leading to enhanced fluctuations when incorporated through the trap factor

$$P_{ij} = \begin{cases} c \left( 1 + a(r_{ij}/R)^2 - b(r_{ij}/R)^4 \right) & \text{when } r_{ij} \leq R, \\ 0 & \text{when } r_{ij} > R, \end{cases} \quad (5.14)$$

in our model. We have chosen  $a$  as the free parameter, with  $b = 1 + a$  and  $c = 4(1+a)/[4(1+a) + a^2]$  for normalization. Thus, at a sufficiently high overall temperature  $T = 1/\beta$ , the central part simply melts and loses its superfluid properties, as is also indicated by the vanishing of the modified helicity modulus in Figure 5.6.

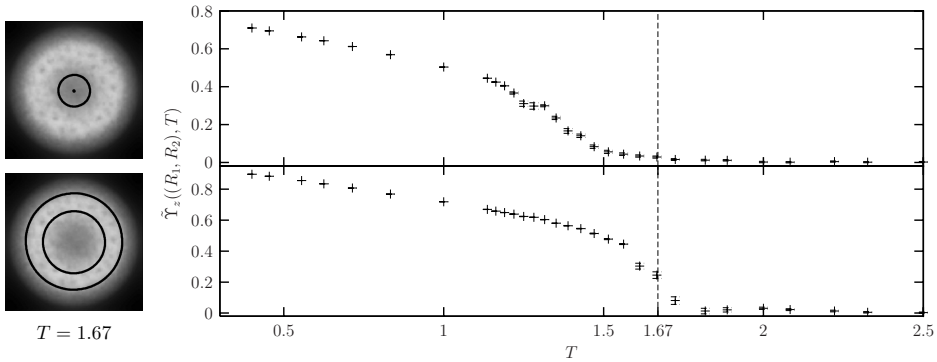


**Figure 5.6:** Modified helicity modulus  $\tilde{\Upsilon}_z$  in a system with a harmonic plus quartic density profile, calculated for the radii indicated by the circles in the leftmost pictures.

Finally, we mention briefly that our model possibly can be applied to the currently very active field of crossover of paired fermion systems from the BCS<sup>1</sup> to the Bose–Einstein regime. Recent work of Schunck and coworkers [106] show remarkably similar structures of the condensate when compared to the renormalized density plots of our simulations with a harmonic trap (Figure 5.7). This

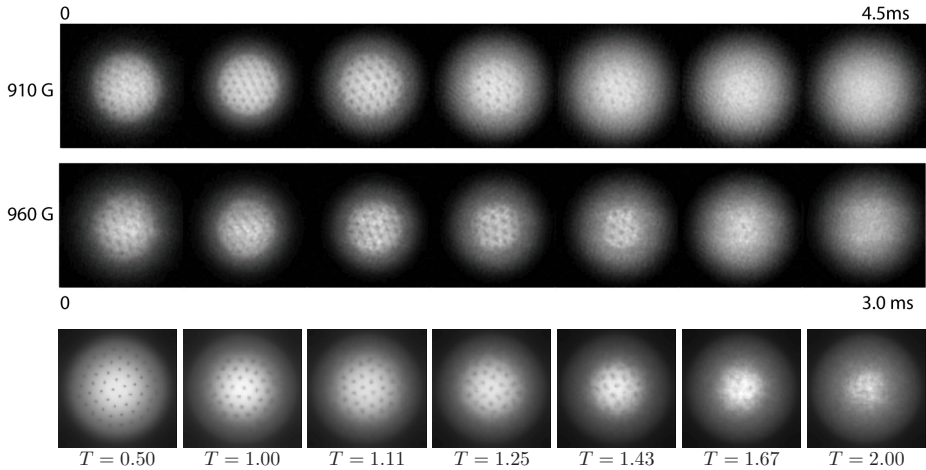


**Figure 5.7:** Observations of vortices in rotating systems where strongly interacting fermions pair up to form a superfluid according to BCS theory (first and second row), after Schunck and coworkers [106]. In the last row, we demonstrate the renormalized condensate density obtained from simulations with a harmonic a priori density profile.

comparison requires further study. It is not clear whether the outer regions of the experimental pictures correspond to unpaired fermions, in which case the  $3DXY$  model does not apply, or fermions in Cooper pairs effectively above the condensation temperature due to low density. In the latter situation, the similarities in Figure 5.7 may not be incidental.

<sup>1</sup>BCS refers to the Bardeen–Cooper–Schrieffer theory for superconductivity.

## Bibliography

- [1] S. Kragset, A. Sudbø, and F. S. Nogueira, Phys. Rev. Lett. **92**, 186403 (2004).
- [2] K. Børkje, S. Kragset, and A. Sudbø, Phys. Rev. B **71**, 085112 (2005).
- [3] S. Kragset, E. Smørgrav, J. Hove, F. S. Nogueira, and A. Sudbø, cond-mat/0609336 , submitted to Phys. Rev. Lett.
- [4] S. Kragset, E. Babaev, and A. Sudbø, cond-mat/0604416 , accepted for publication in Phys. Rev. Lett.
- [5] A. K. Nguyen, *Phase transitions in extreme type-II superconductors: topological defects, and dual description of the vortex system*, PhD thesis, NTNU, 1999.
- [6] S. Mo, *Phase structure and critical properties of an abelian gauge theory*, PhD thesis, NTNU, 2001.
- [7] J. Hove, *Critical properties of the Abelian Higgs model*, PhD thesis, NTNU, 2002.
- [8] J. Smiseth, *Criticality and novel quantum liquid phases in Ginzburg–Landau theories with compact and non-compact gauge fields*, PhD thesis, NTNU, 2005.
- [9] E. Smørgrav, *Critical properties of effective gauge theories for novel quantum fluids*, PhD thesis, NTNU, 2005.
- [10] R. K. Pathria, *Statistical Mechanics, Second Edition* (Butterworth-Heinemann, 1996).
- [11] P. M. Chaikin and T. C. Lubensky, *Principles of condensed matter physics* (Cambridge University Press, 2000).
- [12] N. Goldenfeld, *Lectures on phase transitions and the renormalization group* (Addison-Wesley Publishing Company, 1992).
- [13] A. Sudbø, E. Smørgrav, J. Smiseth, F. S. Nogueira, and J. Hove, Phys. Rev. Lett. **89**, 226403 (2002).

- [14] J. Smiseth, E. Smørgrav, F. S. Nogueira, J. Hove, and A. Sudbø, *Phys. Rev. B* **67**, 205104 (2003).
- [15] H. E. Stanley, *Introduction to phase transitions and critical phenomena* (Clarendon Press Oxford, 1971).
- [16] V. Berezinskii, *Sov. Phys. JETP* **32**, 493 (1970).
- [17] J. M. Kosterlitz and D. J. Thouless, *J. Phys. C* **6**, 1181 (1973).
- [18] D. P. Landau and K. Binder, *A guide to monte carlo simulations in statistical physics* (Cambridge University Press, Cambridge, 2000).
- [19] L. D. Landau and E. M. Lifshitz, *Statistical physics, 2nd edition* (Pergamon Press, Oxford, 1969).
- [20] V. L. Ginzburg, *Sov. Phys. JETP* **4**, 153 (1957).
- [21] J. B. Kogut, *Rev. Mod. Phys.* **51**, 659 (1979).
- [22] A. K. Nguyen and A. Sudbø, *Phys. Rev. B* **60**, 15307 (1999).
- [23] N. D. Mermin and H. Wagner, *Phys. Rev. Lett.* **17**, 1307 (1966).
- [24] R. Savit, *Rev. Mod. Phys.* **52**, 453 (1980).
- [25] H. Kleinert, *Gauge fields in condensed matter physics, Vol. 1* (World Scientific, Singapore, 1989).
- [26] M. B. Einhorn and R. Savit, *Phys. Rev. D* **17**, 2583 (1978).
- [27] J.-R. Lee and S. Teitel, *Phys. Rev. B* **46**, 3247 (1992).
- [28] L. Onsager, *Phys. Rev.* **65**, 117 (1944).
- [29] W. K. Hastings, *Biometrika* **57**, 97 (1970).
- [30] N. Metropolis, A. W. Rosenbluth, M. N. Rosenbluth, A. H. Teller, and E. Teller, *J. Chem. Phys.* **21**, 1087 (1953).
- [31] B. A. Berg and T. Neuhaus, *Phys. Rev. Lett.* **68**, 9 (1992).
- [32] B. A. Berg, *Comput. Phys. Commun.* **153**, 397 (2003).
- [33] J. J. Binney, N. J. Dowrick, A. J. Fisher, and M. E. J. Newman, *The theory of critical phenomena, an introduction to the renormalization group* (Oxford University Press, Oxford, 1992).

- [34] A. M. Ferrenberg and R. H. Swendsen, Phys. Rev. Lett. **61**, 2635 (1988).
- [35] A. M. Ferrenberg and R. H. Swendsen, Phys. Rev. Lett. **63**, 1195 (1989).
- [36] K. Kajantie, L. Kärkkäinen, and K. Rummukainen, Nucl. Phys. B **333**, 100 (1990).
- [37] J. Hove, Phys. Rev. E **70**, 056707 (2004).
- [38] B. A. Berg, Comput. Phys. Commun. **69**, 7 (1992).
- [39] K. G. Wilson, Rev. Mod. Phys. **47**, 773 (1975).
- [40] P. W. Anderson, *Basic notions of condensed matter physics* (Benjamin/Cummings, 1984).
- [41] B. Widom, The Journal of Chemical Physics **43**, 3892 (1965).
- [42] M. Campostrini, M. Hasenbusch, A. Pelissetto, P. Rossi, and E. Vicari, Phys. Rev. B **63**, 214503 (2001).
- [43] H. Weber and P. Minnhagen, Phys. Rev. B **37**, 5986 (1988).
- [44] P. Olsson and P. Holme, Phys. Rev. B **63**, 052407 (2001).
- [45] J.-R. Lee and S. Teitel, Phys. Rev. Lett. **64**, 1483 (1990).
- [46] J. Lidmar and M. Wallin, Phys. Rev. B **55**, 522 (1997).
- [47] P. Minnhagen and B. J. Kim, Physical Review B **67**, 172509 (2003).
- [48] M. E. Fisher and A. N. Berker, Phys. Rev. B **26**, 2507 (1982).
- [49] J. L. Cardy and P. Nightingale, Phys. Rev. B **27**, 4256 (1983).
- [50] J. Lee and J. M. Kosterlitz, Phys. Rev. Lett. **65**, 137 (1990).
- [51] J. Lee and J. M. Kosterlitz, Phys. Rev. B **43**, 3265 (1991).
- [52] H. Kleinert, F. S. Nogueira, and A. Sudbø, Phys. Rev. Lett. **88**, 232001 (2002).
- [53] H. Kleinert, F. S. Nogueira, and A. Sudbø, Nucl. Phys. B **666**, 361 (2003).
- [54] J. Bardeen, L. N. Cooper, and J. R. Schrieffer, Phys. Rev. **108**, 1175 (1957).
- [55] S. Sachdev, Reviews of Modern Physics **75**, 913 (2003).
- [56] J. B. Marston and I. Affleck, Phys. Rev. B **39**, 11538 (1989).

- [57] P. A. Lee and N. Nagaosa, Phys. Rev. B **46**, 5621 (1992).
- [58] N. Nagaosa and P. A. Lee, Phys. Rev. B **61**, 9166 (2000).
- [59] E. Fradkin and S. H. Shenker, Phys. Rev. D **19**, 3682 (1979).
- [60] A. M. Polyakov, Nucl. Phys. B **120**, 429 (1977).
- [61] M. B. Einhorn and R. Savit, Phys. Rev. D **19**, 1198 (1979).
- [62] I. Ichinose and T. Matsui, Phys. Rev. B **51**, 11860 (1995).
- [63] I. Ichinose, T. Matsui, and M. Onoda, Phys. Rev. B **64**, 104516 (2001).
- [64] I. F. Herbut and B. H. Seradjeh, Physical Review Letters **91**, 171601 (2003).
- [65] I. F. Herbut, B. H. Seradjeh, S. Sachdev, and G. Murthy, Physical Review B **68**, 195110 (2003).
- [66] M. J. Case, B. H. Seradjeh, and I. F. Herbut, Nucl. Phys. B **676**, 572 (2004).
- [67] M. N. Chernodub, E. M. Ilgenfritz, and A. Schillerd, Phys. Lett. B **547**, 269 (2002).
- [68] M. N. Chernodub, E. M. Ilgenfritz, and A. Schillerd, Phys. Lett. B **555**, 206 (2003).
- [69] Y. Saito and H. Müller-Krumbhaar, Phys. Rev. B **23**, 308 (1981).
- [70] P. Minnhagen and M. Wallin, Phys. Rev. B **36**, 5620 (1987).
- [71] P. Gupta and S. Teitel, Phys. Rev. B **55**, 2756 (1997).
- [72] P. Minnhagen, Rev. Mod. Phys. **59**, 1001 (1987).
- [73] J. Fröhlich and T. Spencer, J. Stat. Phys. **24**, 617 (1981).
- [74] S. Sachdev, Quantum phases and phase transitions of mott insulators, in *Lecture Notes in Physics: Quantum magnetism*, edited by U. Schollwock, J. Richter, D. J. J. Farnell, and R. A. Bishop, Springer, Berlin, 2004.
- [75] T. Senthil, L. Balents, S. Sachdev, A. Vishwanath, and M. P. A. Fisher, **303**, 1490 (2004).
- [76] T. Senthil, L. Balents, S. Sachdev, A. Vishwanath, and M. P. A. Fisher, Phys. Rev. B **70**, 144407 (2004).

- [77] M. V. Berry, *Physics Today* **43**, 34 (1990).
- [78] F. D. M. Haldane, *Phys. Rev. Lett.* **61**, 1029 (1988).
- [79] E. Dagotto, *Rev. Mod. Phys.* **66**, 763 (1994).
- [80] E. Babaev, *Phys. Rev. Lett.* **89**, 067001 (2002).
- [81] E. Babaev, *Nuclear Physics B* **686**, 397 (2004).
- [82] J. Smiseth, E. Smørgrav, E. Babaev, and A. Sudbø, *Phys. Rev. B* **71**, 214509 (2005).
- [83] E. Babaev, A. Sudbø, and N. W. Ashcroft, *Nature* **431**, 666 (2004).
- [84] O. I. Motrunich and A. Vishwanath, *Phys. Rev. B* **70**, 075104 (2004).
- [85] G. Baym, C. Pethick, and D. Pines, *Nature* **224**, 673 (1969).
- [86] E. J. Yarmchuk, M. J. V. Gordon, and R. E. Packard, *Phys. Rev. Lett.* **43**, 214 (1979).
- [87] A. Houghton, R. A. Pelcovits, and A. Sudbø, *Phys. Rev. B* **40**, 6763 (1989).
- [88] G. Blatter, M. V. Feigel'man, V. B. Geshkenbein, A. I. Larkin, and V. M. Vinokur, *Rev. Mod. Phys.* **66**, 1125 (1994).
- [89] E. Smørgrav, J. Smiseth, E. Babaev, and A. Sudbø, *Phys. Rev. Lett.* **94**, 096401 (2005).
- [90] Y.-H. Li and S. Teitel, *Phys. Rev. Lett.* **66**, 3301 (1991).
- [91] R. E. Hetzel, A. Sudbø, and D. A. Huse, *Phys. Rev. Lett.* **69**, 518 (1992).
- [92] X. Hu, S. Miyashita, and M. Tachiki, *Phys. Rev. Lett.* **79**, 3498 (1997).
- [93] J. R. Abo-Shaeer, C. Raman, J. M. Vogels, and W. Ketterle, *Science* **292**, 476 (2001).
- [94] A. A. Abrikosov, *Zh. Eksp. Teor. Fiz.* **32**, 1442 (1957).
- [95] M. H. Anderson, J. R. Ensher, M. R. Matthews, C. E. Wieman, and E. A. Cornell, *Science* **269**, 198 (1995).
- [96] K. B. Davis *et al.*, *Phys. Rev. Lett.* **75**, 3969 (1995).
- [97] V. Schweikhard, I. Coddington, P. Engels, V. P. Mogendorff, and E. A. Cornell, *Physical Review Letters* **92**, 040404 (2004).



## Bibliography

---

- [98] V. Bretin, S. Stock, Y. Seurin, and J. Dalibard, *Physical Review Letters* **92**, 050403 (2004).
- [99] L. J. Campbell and R. M. Ziff, *Phys. Rev. B* **20**, 1886 (1979).
- [100] C. Pethick and H. Smith, *Bose-Einstein Condensation in Dilute Gases* (Cambridge University Press, 2001).
- [101] A. J. Leggett, *Rev. Mod. Phys.* **73**, 307 (2001).
- [102] N. R. Cooper, S. Komineas, and N. Read, *Physical Review A* **70**, 033604 (2004).
- [103] G. Watanabe, G. Baym, and C. J. Pethick, *Physical Review Letters* **93**, 190401 (2004).
- [104] [http://cua.mit.edu/ketterle\\_group](http://cua.mit.edu/ketterle_group).
- [105] S. Kragset, E. Babaev, and A. Sudbø, unpublished .
- [106] C. H. Schunck, M. W. Zwierlein, A. Schirotzek, and W. Ketterle, *cond-mat/0607298* (2006).